Cranial osteology of the Early Cretaceous turtle *Pleurosternon bullockii* (Paracryptodira: Pleurosternidae)

Serjoscha W Evers [Corresp., 1] , **Yann Rollot** [1] , **Walter G Joyce** [1]

[1] Department of Geosciences, University of Fribourg, Fribourg, Switzerland

Corresponding Author: Serjoscha W Evers
Email address: serjoscha.evers@googlemail.com

Pleurosternon bullockii is a turtle from the Early Cretaceous of Europe known from numerous postcranial remains. Only one skull has so far been referred to the species. *Pleurosternon bullockii* belongs to a group of turtles called pleurosternids, which is thought to include several poorly known taxa from the Late Jurassic and Early Cretaceous of Europe and North America. Pleurosternids and baenids, a group of North American turtles that lived from the Late Cretaceous to the Eocene, define a clade called Paracryptodira. Additionally, Paracryptodira likely includes compsemydids, and, potentially, helochelydrids. Character support for Paracryptodira is relatively weak, and many global phylogenetic studies fail to support paracryptodiran monophyly altogether. Proposed paracryptodiran synapomorphies are largely cranial, despite the poor characterization of pleurosternid cranial material. In addition to their questionable monophyly, the global position of paracryptodires is debated. Early studies suggest crown-turtle affinities, but most phylogenies find them as stem-turtles, irrespective of their monophyly. Here, we document the cranial osteology of *Pleurosternon bullockii* with the use of three-dimensional models derived from segmenting high-resolution X-ray micro-computed tomography (CT) scans. *Pleurosternon bullockii* has a primitive basipterygoid region of the skull, but a cryptodire-like acustico-jugular region. A surprising number of similarities with pleurodires exist, particularly in the laterally expanded external process of the pterygoid and in the posterior orbital wall. Our observations constitute an important step toward a phylogenetic re-evaluation of Paracryptodira.

1 **Cranial osteology of the Early Cretaceous turtle *Pleurosternon***

2 ***bullockii* (Paracryptodira: Pleurosternidae)**

4 Serjoscha W. Evers[1], Yann Rollot[1] and Walter G. Joyce[1]

6 [1]Department of Geosciences, University of Fribourg, Fribourg, Switzerland

8 Corresponding Author:

9 Serjoscha W. Evers[1]

10 Chemin de Musée 6, 1700 Fribourg, Switzerland

11 Email address: serjoscha.evers@unifr.ch

13 **ABSTRACT**

14 *Pleurosternon bullockii* is a turtle from the Early Cretaceous of Europe known from numerous

15 postcranial remains. Only one skull has so far been referred to the species. *Pleurosternon*

16 *bullockii* belongs to a group of turtles called pleurosternids, which is thought to include several

17 poorly known taxa from the Late Jurassic and Early Cretaceous of Europe and North America.

18 Pleurosternids and baenids, a group of North American turtles that lived from the Late

19 Cretaceous to the Eocene, define a clade called Paracryptodira. Additionally, Paracryptodira

20 likely includes compsemydids, and, potentially, helochelydrids. Character support for

21 Paracryptodira is relatively weak, and many global phylogenetic studies fail to support

22 paracryptodiran monophyly altogether. Proposed paracryptodiran synapomorphies are largely

23 cranial, despite the poor characterization of pleurosternid cranial material. In addition to their

24   questionable monophyly, the global position of paracryptodires is debated. Early studies suggest

25   crown-turtle affinities, but most phylogenies find them as stem-turtles, irrespective of their

26   monophyly. Here, we document the cranial osteology of *Pleurosternon bullockii* with the use of

27   three-dimensional models derived from segmenting high-resolution X-ray micro-computed

28   tomography (CT) scans. *Pleurosternon bullockii* has a primitive basipterygoid region of the

29   skull, but a cryptodire-like acustico-jugular region. A surprising number of similarities with

30   pleurodires exist, particularly in the laterally expanded external process of the pterygoid and in

31   the posterior orbital wall. Our observations constitute an important step toward a phylogenetic

32   re-evaluation of Paracryptodira.

34   Key words: Testudines, Paracryptodira, Pleurosternidae, Baenidae, systematics, turtles

36   **INTRODUCTION**

37   Paracryptodires are often referred to as 'one of the three primary clades of (crown) turtles' (e.g.

38   Joyce, 2017). This assessment is primarily based on unresolved phylogenetic positions between

39   Pleurodira, Cryptodira, and Paracryptodira among early global phylogenetic studies (e.g. Joyce,

40   2007). However, most recent phylogenetic analyses recover paracryptodires as stem-turtles, just

41   outside of the turtle crown (e.g. Sterli, 2010; Rabi et al., 2014; Cadena & Parham, 2015; Zhou &

42   Rabi, 2015; Joyce et al., 2016; Evers & Benson, 2019). Paracryptodires were originally defined

43   as a group of turtles that includes baenids, pleurosternids (including 'Glyptopsidae' of Gaffney,

44   1972), *Compsemys victa*, and *Kallokibotion bajazidi* (Gaffney, 1975a). Although only one

45   formal phylogenetic analysis has since found these exact turtles in a monophyletic group (a

46   Lyson & Joyce, 2011 analysis of the matrix of Gaffney et al., 2007), a sister relationship of

47   baenids with pleurosternids has been found frequently (e.g., Gaffney et al., 2007; Joyce, 2007;

48   Lyson & Joyce, 2011; Pérez-García, Royo-Torres & Cobos, 2015; Joyce et al, 2016; Joyce &

49   Rollot, in press). As a consequence, most authors associate the term 'Paracryptodira' with a

50   clade that either exclusively includes baenids and pleurosternids (e.g. Joyce, 2007), or a clade

51   that minimally includes these clades, variously joined by compsemydids, helochelydrids, or

52   indeterminate paracryptodiran taxa (Lyson & Joyce, 2011). Lyson & Joyce (2011) formalized

53   this notion of Paracryptodira by coining a stem-based phylogenetic definition that includes

54   *Pleurosternon bullockii* and *Baena arenosa* as its internal specifiers. Character support for

55   Paracryptodira is relatively weak. The main osteological feature that has historically been used to

56   unite paracryptodires is a far anteriorly positioned foramen for the entry of the internal carotid

57   artery (foramen posterius canalis carotici interni; Rabi et al., 2013) formed midway along the

58   parabasisphenoid-pterygoid suture (Gaffney, 1975a). This feature persists to be cited as

59   diagnostic for paracryptodires (see review of Joyce & Anquetin, 2019), although the foramen has

60   repeatedly been interpreted to be absent altogether in at least some paracryptodires (Sterli et al.,

61   2010; Rabi et al., 2013; Anquetin & André, 2020). Additionally, many of the other originally

62   proposed characters in support of the group are symplesiomorphically present in Testudinata

63   (e.g. presence of nasal, reduced prefrontal exposure on skull roof, presence of mesoplastra,

64   presence of paired gular scutes; Gaffney, 1975a). Some proposed synapomorphies, such as the

65   reduction of the palatine artery (Gaffney, 1975a) or a reduced fenestra perilymphatica (Joyce,

66   2007), are, similar to the aforementioned position of the foramen posterius canalis carotici interni

67   midway along the parabasisphenoid-pterygoid suture (Gaffney, 1975a; Joyce & Anquetin, 2019),

68   not universally present in paracryptodires (e.g. Anquetin & André, 2020; this study) and should

69   thus be re-evaluated on a broader scale. Ambiguity in character support of Paracryptodira is also

70   implicit from many global phylogenetic studies that fail to retrieve the constituent taxa as

71   monophyletic altogether (Sterli, 2010; Anquetin, 2012; Sterli, Pol & Laurin, 2013; Cadena &

72   Parham, 2015; Rabi et al., 2014; Zhou & Rabi, 2015; Joyce et al., 2016; Evers & Benson, 2019).

73   Although most frequently cited paracryptodiran synapomorphies are cranial characters, non-

74   baenid paracryptodiran skulls are poorly known (Joyce & Anquetin, 2019). Five taxa have

75   relatively complete skulls, including the compsemydid *Compsemys victa* (Lyson & Joyce, 2011),

76   the indeterminate paracryptodire *Uluops uluops* (Carpenter & Bakker, 1990), and the

77   pleurosternids *Glyptops ornatus* (Gaffney, 1979a), *Dorsetochelys typocardium* (Evans & Kemp,

78   1976) and *Pleurosternon bullockii* (Evans & Kemp, 1975). Here, we re-examine UMZC T1041,

79   the cranium of *Pleurosternon bullockii* that was originally described as *Mesochelys durlstonensis*

80   by Evans & Kemp (1975), based on high-resolution micro-computed tomography (CT) scanning.

81   We describe the cranium in detail and compare it to available material of other paracryptodires,

82   and, where relevant, other groups of turtles. Thorough anatomical characterizations like the one

83   presented here form the base work for phylogenetic assessments. Our description and

84   comparisons provide anatomical evidence for unique morphologies of pleurosternids, which

85   likely include at least *Uluops uluops* besides *Pleurosternon bullockii* and *Glyptops ornatus*.

86   Pleurosternids show a mixture of plesiomorphic and derived features, tentatively supporting their

87   inferred position as stem-taxa that are relatively close to the crown-node of turtles. We hope that

88   our descriptions lead to the coding of novel phylogenetic characters, that further scrutinize the

89   monophyly and global position of paracryptodires.

90

91   **MATERIAL & METHODS**

92   High-resolution X-ray computed tomography (CT) scans were obtained for the cranium of

93   UMZC T1041, which is the holotype of *Mesochelys durlstonensis* Evans & Kemp, 1975. UMZC

94   T1041 was found in the Early Cretaceous (Berriasian) Purbeck Limestone Group in Durlston

95   Bay, United Kingdom (Evans & Kemp, 1975). Gaffney & Meylan (1988) referred the material to

96   *Pleurosternon bullockii* Owen, 1842, albeit without justification. Milner (2004) compared the

97   shell remains associated with the cranium of *Mesochelys durlstonensis* with those of

98   *Pleurosternon bullockii*, and presented anatomical evidence for the synonymy suggested by

99   Gaffney & Meylan (1988). This has generally been accepted ever since (see review of Joyce &

100   Anquetin, 2019). Scans of UMZC T1041 were obtained by Roger Benson in 2017 at the

101   Cambridge Biotomography Center, using a X-Tek H 225 μCT scanner (Nikon Metrology, Tring,

102   UK). The cranium was scanned using a beam energy of 130 kV, a current of 250 μA, 500 ms

103   exposure time, 1 frame per 1400 projections, and no filter, resulting in a voxel size of 0.03315

104   mm. The resulting CT-scans were segmented in the software Mimics (v. 16.0–19.0;

105   http://biomedical.materialise.com/mimics), and 3D models were exported as .ply files. Figures of

106   digital renderings were compiled using the software Blender v. 2.71 (blender.org). CT-slice data

107   as well as the 3D models are deposited at MorphoSource (Evers, 2020).

108   We mostly compare UMZC T1041 to a selection of likely paracryptodires from the Late

109   Jurassic to Cretaceous of North America and Europe based on description published in the

110   literature, in particular *Arundelemys dardeni* (as described by Lipka et al., 2006), *Compsemys*

111   *victa* (as described by Lyson & Joyce, 2011), *Dorsetochelys typocardium* (as described by Evans

112   & Kemp, 1976 under the name *Dorsetochelys delairi*), *Eubaena cephalica* (as described by

113   Rollot, Lyson & Joyce, 2018), *Glyptops ornatus* (as described by Gaffney, 1979a under the name

114   *Glyptops plicatulus*), and *Uluops uluops* (as described by Carpenter & Bakker, 1990). For

115   comparisons with *Dorsetochelys typocardium*, we used a 3D model of the holotype (DORCM

116   G.00023) that was made available under a CC-BY-NC-SA license by the "GB3D Type Fossils"

117   projects hosted by the British Geological Survey at www.3d-fossils.ac.uk. The descriptions of

118   *Compsemys victa* (based on UCM 53971) and *Uluops uluops* (based on UCM 49223) were

119   complemented by CT scans of these specimens. The original descriptions are cited for all

120   previously described features, but the specimen numbers are cited when novel observations

121   regarding these taxa are made based on these scans. These scans will be further discussed and

122   made public in a forthcoming paper.

123

124   **DESCRIPTION**

125   **General comments.** The cranium of UMZC T1041 disarticulated into several blocks of fully to

126   partially articulated bones, which were then displaced to give the skull a crushed appearance

127   (Figs. 1, 2). The 3D anatomy of individual bones is nevertheless near perfect. For instance, the

128   left pterygoid, prootic, opisthotic, quadrate, and the parabasisphenoid form a block in which

129   these bones are still mostly preserved in their original positions relative to one another. The

130   parabasisphenoid, however, is shifted medially relative to the pterygoid.

131   The skull of UMZC T1041 is relatively low dorsoventrally, relatively narrow mediolaterally,

132   but elongate anteroposteriorly (Figs. 1, 2). The orbits face more laterally than in *Glyptops*

133   *ornatus* (Gaffney, 1979a), but less so than in *Compsemys victa* (Lyson & Joyce, 2011). The

134   entire skull roof and lateral side of the skull of UMZC T1041 is covered by the dense surface

135   sculpturing that is characteristic of many paracryptodires (e.g., Pérez-García, 2014; Joyce &

136   Lyson, 2015; Joyce & Anquetin, 2019). Although superficially the surface sculpturing of

137   paracryptodires is very similar among species, some differences can be made out. For instance,

138   although the main textural element in both *Uluops uluops* (Carpenter & Bakker, 1990; UCM

139   53971) and *Pleurosternon bullockii* (UMZC T1041) are small and irregular tubercles, these

140   transition into a ridge-like arrangement on the posterior margin of the parietal in UMZC T1041

141   (Fig. 2A), but not in *Uluops uluops* (UCM 53971). The skull emarginations of UMZC T1041 are

142   moderately developed: the cheek emargination is relatively deep, reaching about mid-orbit in

143   lateral view. The jugal and quadratojugal margins are strongly concave and the maxilla and

144   quadrate are included in the emargination (Fig. 2C–D). The same morphology is seen in *Uluops*

145   *uluops* (UCM 53971). The medial portion of the upper temporal emargination of UMZC T1041

146   is visible as a concavity developed along the posterior margin of the parietal that exposes only a

147   small part of the floor of the adductor chamber (Fig. 2A), again as in *Uluops uluops* (UCM

148   53971). The lateral portions of the upper temporal emargination that were likely formed by the

149   squamosal are damaged. Squamosal and supraoccipital crests are comparatively strongly

150   developed, providing elongate attachment sites for the adductor musculature.

151

152   **Nasal.** Only the left nasal of UMZC T1041 is preserved (Fig. 2A, C, E). However, as the left

153   nasal is in articulation with the frontal, prefrontal, and maxilla on the left side, the anterior region

154   of the skull roof can be completely reconstructed. The nasal is a triangular element that tapers

155   posteriorly and inserts into a gap between the prefrontal and frontal. The long anterior frontal

156   processes separate the paired nasals posteriorly, but anteriorly a short nasal-nasal suture can be

157   inferred, which is generally present in basal paracryptodires (Gaffney, 1972; Lyson & Joyce,

158   2015; Joyce & Anquetin, 2019).

159

160   **Prefrontal.** Both prefrontals of UMZC T1041 are preserved (Fig. 2). The prefrontal has a small

161   skull roof exposure in UMZC T1041, and is restricted to a small area at the anterodorsal orbital

162   margin, contacting the nasal, frontal, and maxilla. Evans & Kemp (1975) also reported a contact

163   with the vomer. The relevant part of the specimen has since been lost, but the side of the

164   descending process makes this contact highly plausible. Medially, the frontals hinder both

165   prefrontals from a mutual contact. Anterolaterally, the prefrontal has a deep vertical groove for

166   the reception of the ascending process of the maxilla, which is partially exposed on both sides

167   due to partial disarticulation. However, on the left side, the maxilla and prefrontal are articulated

168   enough to see that a small foramen orbito-nasale was laterally and dorsally framed by both

169   bones. As the vomer and palatine bones are absent, the medial margin of the foramen is

170   unknown. However, the foramen was medially probably closed by the palatine, as in *Uluops*

171   *uluops* (UCM 53971).

172

173   **Frontal.** Both frontals are preserved (Fig. 2). The frontal contacts the nasal, prefrontal,

174   postorbital, and parietal. The frontal is a relatively elongate, but narrow bone in UMZC T1041:

175   the anterior portion forms long and narrow processes that divide the internasal contact for half of

176   the nasal length (Fig. 2A). A process that partially separates the nasals is only slightly present in

177   *Dorsetochelys typocardium* (Evans & Kemp, 1976) and *Arundelemys dardeni* (Lipka et al.,

178   2006), but otherwise generally absent in other paracryptodires, such as *Glyptops ornatus*

179   (Gaffney, 1979a), *Compsemys victa* (Lyson & Joyce, 2011), or baenids (Gaffney,1972; Joyce &

180   Lyson, 2015). The frontal contributes to the orbit in UMZC T1041 by means of a broad lateral

181   process (Fig. 2A). Ventrally, both frontals form a narrow sulcus olfactorius that extends

182 anteriorly into the fossa nasalis (Fig. 3). The right and left crista cranii diverge posteriorly from

183 the midline and become shallower near the suture with the parietal.

184

185 **Parietal.** Both parietals are preserved in UMZC T1041 (Fig. 2). The parietal forms the posterior

186 and central parts of the skull roof and contacts the frontal anteriorly, the postorbital laterally, and

187 almost certainly the squamosal posterolaterally. Ventrally, the parietal contacts the

188 supraoccipital, prootic, epipterygoid, and possibly the pterygoid (Fig. 4B). The parietal forms a

189 tapering posteromedian process, which seems to have covered the supraoccipital entirely (see

190 supraoccipital). The posterior margin of the parietal is emarginated lateral to the midline, but still

191 conceals most of the otic capsule in dorsal view (Fig. 2A), as is also the case in *Dorsetochelys*

192 *typocardium* (Evans & Kemp, 1976) and *Uluops uluops* (UCM 53971). The right parietal of

193 UMZC T1041 is broken posterolaterally near the squamosal, so that the contact between these

194 bones is not preserved. However, if the right squamosal were a mirror image of the one on the

195 left side, where the squamosal is missing but the parietal completely preserved, both bones

196 would clearly have a short contact posterior to the postorbital. A squamosal-parietal contact is

197 also present in *Dorsetochelys typocardium* (Evans & Kemp, 1976) and *Uluops uluops* (UCM

198 53971).

199   The descending process of the parietal is well-developed in UMZC T1041 (Figs. 3, 4B),

200 although the anterior margin of the process is posteriorly retracted, so that the interorbital

201 fenestra is large. Internally, the medial surface of the base of the descending process seems

202 bulged within the endocranial cavity, suggesting that *Pleurosternon bullockii* possibly had large

203 cerebral hemispheres. The posteroventral margin of the descending process of the parietal

204 contacts the supraoccipital posteriorly and the prootic anteriorly. At the dorsal margin of the

205   trigeminal foramen, the parietal forms a thin posteroventral process that also frames the posterior

206   margin of the foramen, and extends to contact the pterygoid, thereby excluding the prootic from

207   contributing to the foramen (Fig. 4). This is visible on the right side of UMZC T1041, where the

208   prootic, parietal, quadrate, and partially the pterygoid and epipterygoid are preserved in

209   articulation. The same arrangement can be observed in *Uluops uluops* (UCM 53971) at the

210   posterior margin of the trigeminal foramen. A posteroventral process of the parietal along the

211   posterior trigeminal foramen margin has been proposed as a synapomorphy of Thalassochelydia

212   (Anquetin, Püntener & Joyce, 2017), based on the presence of this process in *Solnhofia parsonsi*

213   and plesiochelyids (Anquetin, Püntener & Billon-Bruyat, 2015). The same process has also been

214   observed in sandownids (Evers & Joyce, 2020). The presence of this process in paracryptodires

215   as well as the aforementioned groups, all of which have recently been interpreted as stem-turtles

216   (e.g. Evers & Benson, 2019), indicates that this could be a feature that is more widespread along

217   the crownward stem-lineage of turtles. The contacts of the parietal of UMZC T1041

218   anteroventral to the trigeminal foramen are not clearly preserved on either side of the specimen.

219   However, contacts with both the epipterygoid and pterygoid were likely present.

220   Most of the lateral contact with the postorbital is formed as a simple, planar contact without

221   further reinforcement. However, at the level of the base of the descending process, the parietal

222   expands laterally underneath the postorbital (Fig. 3). The ventral surface of this buttress is

223   hypertrophied to a mediolateral ridge between the descending process of the parietal and the

224   ventral process of the postorbital. This shallow ridge forms the posterior boundary of a shallow

225   fossa that is anteriorly bound by the medial margin of the orbital fossa, and which we identify as

226   as the roof to the sulcus palatino-pterygoideus (see postorbital). The same fossa is also present in

227   various other turtle, though rarely reported, we note that it is particularly deep in UMZC T1041,

228   *Uluops uluops* (UCM 53971), and pleurodires (Gaffney, Tong, & Meylan, 2006).

229

230   **Postorbital.** Both postorbitals are preserved in UMZC T1041 (Fig. 2). The postorbital contacts

231   the frontal anteromedially, the parietal posteromedially, the squamosal posteriorly, the

232   quadratojugal posteroventrally, and the jugal ventrally.

233   The postorbital of UMZC T1041 is posteriorly elongate (Fig. 2A–D) and forms the extensive

234   temporal roofing together with the parietal. However, the postorbital is excluded from the

235   posterior margin of the skull roof by a squamosal-parietal contact. The postorbital and squamosal

236   contact is located dorsal to the margin of the cavum tympani, but separated from contacting the

237   cavum or quadrate by a posterior process of the quadratojugal (Fig. 2D). The quadratojugal

238   contacts the postorbital posterior to the jugal-postorbital contact.

239   The postorbital forms the posterior margin of the orbit (Fig. 2C–D). Although the preservation

240   of UMZC T1041 leaves a bit of room for interpretation regarding the posterior orbital margin,

241   the jugal was excluded clearly from contributing to the margin of the orbit by a short ventral

242   process of the postorbital that contacted the maxilla (see jugal). Within the orbital fossa, the

243   postorbital forms an expanded ventral process that contacts the medial process of the jugal

244   ventrally (Fig. 3). Hereby, the ventral process of the postorbital nearly contacts the pterygoid,

245   and a contact with the unpreserved palatine cannot be ruled out entirely. The morphology of the

246   ventral process of the postorbital seems to be very similar in *Uluops uluops* (UCM 53971). In

247   this taxon, the postorbital comes close to the pterygoid and palatine, but both contacts are absent.

248   A postorbital-palatine contact is only seen in pleurodires (Gaffney, 1979b). However, the orbito-

249   temporal region of both UMZC T1041 and *Uluops uluops* (UCM 53971) show striking

250 similarities to the morphology of that region in pleurodires: the medial postorbital-jugal

251 expansion forms an extended posterior wall to the orbital fossa (Fig. 3). Additionally, again as in

252 pleurodires, the passage between the temporal fossa posteriorly, and the orbital fossa anteriorly,

253 becomes strongly constricted between the ventral process of the postorbital and the descending

254 process of the parietal (Fig. 3). Furthermore, the roof of this constricted through is depressed to

255 form a shallow fossa (Fig. 3). This morphology is otherwise only found in pleurodires (e.g.

256 Gaffney, Tong & Meylan, 2006). Thus, we use terms from the pleurodire literature to refer to

257 these respective structures; we use 'septum orbitotemporale' for the medial expanded jugal-

258 postorbital wall (Gaffney, Tong & Meylan, 2006: fig. 25), and we use 'sulcus palatino-

259 pterygoideus' for the space between the orbital and temporal fossae (Gaffney, Tong & Meylan,

260 2006: fig. 25), although we note that it is incipient with respect to the pleurodire morphology.

261

262 **Jugal.** Both jugals of UMZC T1041 are preserved (Fig. 2A–D), but the elements are

263 disarticulated slightly from their surrounding bones. Definite contacts are with the postorbital,

264 maxilla, quadratojugal, and pterygoid, and a contact with the palatine cannot be ruled out. The

265 jugal of UMZC T1041 shows typical turtle morphology with a laterally placed, vertical plate that

266 forms part of the lateral skull roof, and a medially directed process that contacts parts of the

267 palate. The jugal is removed from the ventral skull margin, as the maxilla forms a posterior

268 process that extends ventrally underneath the jugal for some distance (Fig. 2C–D). The end of

269 this maxillary process forms the beginning of the moderately deep cheek emargination, which

270 extends from the maxilla along the ventral margins of the jugal and quadratojugal. The dorsally

271 positioned jugal and step-like margin between the maxilla and jugal are also present in *Uluops*

272 *uluops* (UCM 53971), and baenids (Gaffney, 1972), but not so in *Dorsetochelys typocardium*

273 (Evans & Kemp, 1976), in which the jugal is the posterior continuation of the maxilla along the

274 labial margin of the skull.

275 It seems that the jugal was excluded from the orbital margin, as is also the case in *Glyptops*

276 *ornatus* (Gaffney, 1979a), *Arundelemys dardeni* (Lipka et al., 2006), and an assortment of

277 advanced baenids (Gaffney, 1972; Joyce & Lyson, 2015; Rollot, Lyson & Joyce, 2018) as well

278 as helochelydrids (e.g. Joyce et al., 2011; Joyce, Sterli & Chapman, 2014): on both sides, the

279 jugal of UMZC T1041 has an anteriorly recessed surface, which is posteriorly delimited by a

280 rim. Only posteriorly to this rim does the surface of the bones show the sculpturing that covers

281 most of the external bone surfaces (Fig. 2C–D). In *Uluops uluops* (UCM 53971), in which the

282 jugal contributes to the orbit, the surface sculpturing of the jugal bone indeed extends to the

283 orbit. Thus, we interpret the recessed surface in UMZC T1041 to be a laterally exposed facet for

284 the overlying postorbital and maxilla. Our interpretation hereby differs markedly from that of

285 Evans & Kemp (1975), who reconstructed a point contact of the jugal to the orbit margin.

286 Despite its likely exclusion from the orbital margin itself, the jugal of UMZC T1041 is expressed

287 medially to the orbital margin within the orbital fossa, which we call septum orbitotemporale

288 (see postorbital) (Fig. 3). Extending posteromedially from the orbital fossa, the medial process of

289 the jugal reaches the pterygoid. This section of the jugal is ventrally overlain by the maxilla. A

290 contact with the palatine might have been present in this area, but this cannot be confirmed

291 without any indication of the morphology of the palatine bone.

292

293 **Quadratojugal.** The quadratojugal is only preserved on the right side of UMZC T1041 (Fig.

294 2D). The quadratojugal is triradiate, as it forms a posterior process that inserts between the

295 postorbital and quadrate to contact the squamosal, extends ventrally along the anterior quadrate

296   margin, and anteriorly towards the jugal. The quadratojugal of *Pleurosternon bullockii* is a

297   comparatively small bone in comparison to those of basal stem-turtles (e.g., Gaffney, 1990) or

298   baenids (e.g., Joyce and Lyson, 2015; Rollot, Lyson & Joyce, 2018), but not as small as in

299   sichuanchelyids (Sukhanov, 2000; Joyce et al., 2016), which have quadratojugals with a greatly

300   reduced lateral exposure. The quadratojugal of UMZC T1041 is similar in size and extent to that

301   of *Uluops uluops* (UCM 53971). In UMZC T1041, the ventral margin of the quadratojugal

302   contributes to the moderately deep cheek emargination. Although the quadratojugal frames the

303   quadrate anteriorly, it is slightly displaced anteriorly from the margin of the cavum tympani, and

304   clearly does not closely approach the articular condyles of the quadrate.

305

306   **Squamosal.** Only the right squamosal of UMZC T1041 is preserved (Fig. 2). Contacts with the

307   quadratojugal, quadrate, and opisthotic can be documented, and a parietal contact is inferred. The

308   squamosal of *Pleurosternon bullockii* is a large element with a well-developed posterior process

309   and a deeply recessed antrum postoticum. The squamosal caps the posterior part of the quadrate,

310   and hereby forms the posterodorsal margin of the deeply developed cavum tympani, as is also

311   the case in *Uluops uluops* (UCM 53971), *Dorsetochelys typocardium* (Evans & Kemp, 1976),

312   *Compsemys victa* (Lyson & Joyce, 2011), and baenids (Joyce & Lyson, 2015). The squamosal of

313   UMZC T1041 has a deep, incision-like facet for the opisthotic, and thus frames the paroccipital

314   process from dorsal and ventral. Whereas the anterior part of the squamosal is bulbous and

315   houses the expanded antrum postoticum, the bone narrows mediolaterally toward its posterior

316   end to form a vertically sheeted process that extends posteriorly just beyond the level of the

317   supraoccipital crest (Fig. 2A, F).

318

319 **Premaxilla.** Both premaxillae are preserved in UMZC T1041 (Fig. 2A–E). The premaxilla

320 contacts the maxilla, but contacts with the palatine are uncertain due to incomplete preservation.

321 A contact with the vomer was originally preserved (Evans & Kemp, 1975), but the vomer is now

322 lost (see vomer). The right premaxilla completely surrounds a clearly developed foramen

323 praepalatinum (Fig. 2B), which is only incompletely preserved on the other side. The dorsal

324 margin of the premaxilla shows that the external naris was undivided from below in

325 *Pleurosternon bullockii*, as described by Evans & Kemp (1975). Within the nasal fossa, both

326 premaxillae together form a low ridge that probably serves as the insertion for the internarial

327 septum. The full labial ridge, including the premaxillae, frame a broad notch along the midline.

328 Serrations on the premaxillary labial ridge, as reported by Evans and Kemp (1975), are not

329 confirmed for UMZC T1041.

330

331 **Maxilla.** Both maxillae are preserved in UMZC T1041 (Fig. 2A–E). The maxilla contacts the

332 premaxilla anteriorly, the nasal and prefrontal dorsally, the jugal and postorbital posteriorly, and

333 the pterygoid posteromedially. A medial contact with the vomer was previously documented by

334 Evans & Kemp (1975), but is not preserved anymore (see section on the vomer). A contact with

335 the palatine was likely present along the medial margin of the triturating surface. The triturating

336 surface of the maxilla is relatively narrow and lacks a medial ridge (Fig. 2B). The labial ridge is

337 ventrally deep and sharp-edged (Fig. 2B). In anterior view, the labial ridge of the maxilla and

338 premaxilla jointly frame a broad, but shallow median notch (Fig. 2E). A curved labial margin of

339 the maxilla seems common among paracryptodires, although the degree of the curvature varies.

340 UMZC T1041 is intermediate in this regard between *Glyptops ornatus* (Gaffney, 1979a),

341 *Dorsetochelys typocardium* (Evans & Kemp, 1976), and *Arundelemys dardeni* (Lipka et al.,

342   2006) with a weakly curved maxilla on one side, and *Uluops uluops* (UCM 53971) on the other,

343   in which the curvature is very strongly pronounced. The medial margin of the incompletely

344   preserved foramen orbito-nasale of UMZC T1041 is formed by the maxilla, and the foramen

345   alveolaris superior is a comparatively large foramen positioned within that margin (best viewed

346   in the 3D models). Posterior to the ascending process, the maxilla forms the complete ventral

347   margin of the orbit (Fig. 2C–D). The margin is slightly raised to an orbital rim, medial to which

348   the maxilla forms a narrow floor of the orbital fossa. The foramen supramaxillare is small and

349   positioned immediately anterior to the jugal contact within the floor of the orbital fossa (Evans &

350   Kemp, 1975). Posteriorly, the maxilla laterally overlaps the jugal to contact the postorbital along

351   the posterior margin of the orbit (see jugal). The maxilla also extends ventrally to the jugal with a

352   short process (Fig. 2C–D). The posterior part of the maxilla is medially expanded underneath the

353   jugal and reaches the anterior end of the external process of the pterygoid.

354

355   **Vomer.** Evans & Kemp (1975) describe and illustrate a small anterior part of the vomer that was

356   articulated with the premaxillae and the prefrontals. However, this part of the vomer, alongside a

357   small posterior part of the left premaxilla is not preserved in the specimen anymore, and the

358   whereabout of the fragments that must have broken off since the description of Evans & Kemp

359   (1975) are unclear.

360

361   **Palatine.** The palatines are not preserved in UMZC T1041.

362

363   **Quadrate.** Both quadrates of UMZC T1041 are preserved (Fig. 2B–D, F). The quadrate contacts

364   the prootic and opisthotic medially, the pterygoid anteroventrally, the epipterygoid anteriorly, the

365 quadratojugal anterolaterally, and the squamosal posterolaterally. A point contact with the

366 supraoccipital is likely just posterior to the foramen stapedio-temporale. The lateral surface of

367 the quadrate is dominated by the deeply recessed cavity that forms most of the cavum tympani

368 (Fig. 2C–D). The quadrate forms the anterior margin of the cavum tympani, but posterolaterally

369 this structure is formed by the squamosal. The incisura columella auris is posteroventrally open,

370 as in all other paracryptodires (Joyce & Lyson, 2015; Joyce & Anquetin, 2019). The articular

371 process of the quadrate of UMZC T1041 does not protrude ventrally very deep and does not

372 significantly expand beyond the ventral margin of the cavum tympani. Much of the lateral

373 surface of the articular process was probably covered by the ventral ramus of the quadratojugal.

374 In ventral view, the articular surface of the process bears two weakly convex sub-facets (Fig.

375 2B), which are mediolaterally separated by a shallow sulcus (Evans & Kemp, 1975). The medial

376 side of the articular process is buttressed by the posterior process of the pterygoid, but the

377 process does not reach the articular facet (Fig. 2B). Medially, within the cavum acustico-

378 jugulare, the quadrate forms together with the pterygoid and prootic the posterior foramen for the

379 canalis cavernosus. Between the prootic and quadrate, the canalis stapedio-temporalis connects

380 the cavum acustico-jugulare with the adductor chamber (Fig. 5A). The respective exiting

381 foramen, the foramen stapedio-temporale, is formed on the dorsal surface of the otic capsule at

382 the posterior limit of the contact between the quadrate and prootic (Fig. 4A). The foramen and

383 associated canal have a relatively small diameter, superficially similar to trionychians or

384 kinosternoids. However, the diameters of the stapedial and cerebral canals are about equally

385 sized in UMZC T1041, whereas the cerebral artery canal is much larger than the stapedial artery

386 canal in the aforementioned cryptodires. Immediately posterior to the foramen stapedio-

387 temporale of UMZC T1041, the quadrate likely has a short, superficial contact with the

388   supraoccipital, which can also be observed in *Uluops uluops* (UCM 53971) and some baenids

389   like *Stygiochelys estesi* (Gaffney, 1972). Contacts of the quadrate with the opisthotic and

390   squamosal form the posterior aspect of the floor of the adductor chamber in UMZC T1041.

391   Anteriorly within the adductor chamber, the dorsal surface of the quadrate contributes to the

392   formation of the weakly developed processus trochlearis oticum. However, the quadrate forms

393   less of the process than the prootic. The process is developed as a shallowly concave area along

394   the quadrate-prootic contact (Fig. 4A). The processus trochlearis oticum of *Uluops uluops* (UCM

395   53971) is somewhat more pronounced, but otherwise similar to that of *Pleurosternon bullockii*.

396   The anterior quadrate surface of UMZC T1041, ventral to the processus trochlearis oticum,

397   extends anteriorly in a short epipterygoid process (Fig. 4A). This process contacts the

398   epipterygoid but is excluded from the trigeminal foramen margin by a dorsal process of the

399   pterygoid.

400

401   **Epipterygoid.** In UMZC T1041, we identify a small plate-like ossification ventral to the

402   trigeminal foramen as the epipterygoid and thus agree with Evans & Kemp (1975) in the

403   identification of this element. However, the epipterygoids are difficult to segment in our CT

404   scans, due to their highly interdigitated sutures with the parietals, and fragmentation due to

405   breakage in the respective skull area. On the right side of the specimen, the epipterygoid seems

406   to be preserved close to its original position, although its dorsal margin has tipped laterally (Fig.

407   4). Here, the epipterygoid is positioned anteriorly to the epipterygoid process of the quadrate and

408   ventrally to the descending process of the parietal. If the epipterygoid were tilted back into

409   contact with the parietal, it would frame the anteroventral margin of the trigeminal foramen, its

410   usual position (e.g., Gaffney, 1979b). The left epipterygoid, which seems to have been misplaced

411   slightly dorsally, also indicates that a contact with the prootic is likely.

412

413   **Pterygoid.** Both pterygoids of UMZC T1041 are preserved (Fig. 2B). The right pterygoid is

414   basically complete (Fig. 6), but has a transverse break through its center, whereas in the left

415   pterygoid, the external process is broken off but preserved. The pterygoid contacts the

416   parabasisphenoid, jugal, maxilla, parietal, epipterygoid, quadrate, prootic, opisthotic. Although

417   the palatines and the basioccipital are absent, contacts with the pterygoid seem all but certain.

418   However, as the exoccipitals are missing as well, we cannot assess if a pterygoid contact was

419   present with this bone as well. An interpterygoid contact below the rostrum basisphenoidale is

420   certainly absent (see Parabasisphenoid), but a possible midline contact anterior to the

421   parabasisphenoid cannot be ruled out, as the anterior tips of the pterygoids might be damaged.

422   The pterygoid of *Pleurosternon bullockii* shows a mixture of plesiomorphic and derived

423   features, as well as similarities to pleurodires and cryptodires. The general architecture of the

424   bone mimics that of most cryptodires, with a relatively long posterior process that covers large

425   parts of the cavum acustico-jugulare from ventral exposure (Figs. 2B, 5A). The posterior process

426   extends posteriorly up to the tips of the posterior parabasisphenoid processes (= anterior

427   tubercula basioccipitale; see parabasisphenoid), and certainly contacted the basioccipital, as is

428   also the case in *Uluops uluops* (UCM 53971). The posterior pterygoid process of UMZC T1041

429   furthermore completely covers the ventral end of the processus interfenestralis of the opisthotic

430   (Fig. 2B, 5A), as in *Uluops uluops* (UCM 53971) and *Glyptops ornatus* (Gaffney, 1979a). Thus,

431   the process is much more cryptodire-like and extensive than acknowledged in previous

432   descriptions (Evans & Kemp, 1975), although Gaffney (1979a) corrected earlier statements of

433   his, and also argued that in both *Glyptops ornatus* and UMZC T1041 the posterior process of the

434   pterygoid is indistinguishable from cryptodires. Between the articular process of the quadrate

435   and the parabasisphenoid of UMZC T1041, the posterior process of the pterygoid shows a well-

436   developed pterygoid fossa (Figs. 6A, 7C). Despite this cryptodire-like appearance, the pterygoid

437   retains a deep, pocket-like facet on its medial margin for the reception of the basipterygoid

438   processes of the parabasisphenoid (Figs. 6A, 7C). This facet is absent in the crania of all Recent

439   turtles. The medial margin of the pterygoid is laterally curved around the basipterygoid

440   articulation, which results in the formation of a window-like recess in the floor of the

441   basicranium, through which the basipterygoid process of the parabasisphenoid is partially

442   exposed, and through which the cerebral artery and the vidian nerve enter the cranium. The

443   articulation socket for the basipterygoid process within the medial surface of the pterygoid bears

444   a central foramen, which is positioned between the dorsal and ventral flanges of the

445   basipterygoid process (see Parabasisphenoid). The foramen is the entry to the canalis nervus

446   vidianus, which transmits the vidian nerve through the pterygoid towards an anterior foramen

447   that is positioned lateral to the anterior end of the crista pterygoidei (Fig. 6B). The connection of

448   these two foramina and their identification as the canalis nervus vidianus were already correctly

449   inferred by Evans & Kemp (1975), but the foramen within the basipterygoid facet was re-

450   interpreted by Sterli et al. (2010) as the posterior entry foramen of the palatine artery. Our CT

451   scans unambiguously confirm the internal connection of the above-mentioned foramen with the

452   anterior foramen of the canalis nervus vidianus, and thus corroborate the interpretation by Evans

453   & Kemp (1975). Gaffney (1979a) described the presence of a palatine artery canal for *Glyptops*

454   *ornatus* that extends anteriorly from within the basipterygoid articulation socket of the pterygoid,

455   but he could not find an anterior exiting foramen. Thus, it is possible that Gaffney (1979a)

456   misinterpreted the foramen he saw, which could instead be for the vidian nerve canal, and did not

457   find an anterior palatine artery canal foramen, because it does not exist. However, this can only

458   be tested with certainty by attaining CT scans of *Glyptops ornatus*. For UMZC T1041, we can

459   furthermore confirm the canalis pro ramo nervi vidiani of Evans & Kemp (1975; foramen pro

460   ramo nervi vidiani prior to revision of Rollot, Lyson & Joyce [2018]), as a vertically oriented

461   canal that extends through the pterygoid from the floor of the canalis cavernosus to the ventral

462   pterygoid surface posterior to the parabasisphenoid articulation (Fig. 7C). The canalis pro ramo

463   nervi vidiani seems to be present in the same location in *Glyptops ornatus* (Gaffney, 1979a).

464   Immediately anterior to the ventral opening of the canalis pro ramo nervi vidiani of UMZC

465   T1041, a robust ridge surrounds the ventromedial margin of the pterygoid around the

466   basipterygoid facet (Evans & Kemp, 1975). Both the ventral canalis pro ramo nervi vidiani and

467   the robust ridge are affected by the large break of the right pterygoid, but nicely preserved on the

468   left element (Fig. 7C). The ridge persists anteriorly, albeit much more shallowly, parallels the

469   parabasisphenoid suture for a short distance, and curves laterally toward the posteriorly directed

470   tip of the external pterygoid process (Fig. 6A). Evans & Kemp (1975) interpret the ridge to be

471   the insertion for the pterygoideus musculature, and the same ridge morphology is present in

472   *Glyptops ornatus* (Gaffney, 1979a). In *Uluops uluops* (UCM 53971), the pterygoideus muscle

473   ridge is similar, but the ridge traverses the pterygoid earlier and extends to the posterior end of

474   the external process, thus defining a smaller fossa.

475   The external process of the pterygoid is extremely large in UMZC T1041 and projects

476   laterally deeply into the subtemporal fenestra (Figs. 2B, 5A–B, 6). Although many turtles,

477   including many cryptodires (e.g. chelydrids, emydids, geoemydids), have their lateral surface of

478   the external process developed to a vertical flange, this morphology seems hypertrophied in

479   *Pleurosternon bullockii*. The vertical plate of the lateral surface of the external process is less

480   sheeted than in most cryptodires that have the respective flange, but is more robust, and notably

481   gently medially deflected towards its dorsal margin (Fig. 6B–C, 5A–B, 4). As such, the

482   morphology of the external process of the pterygoid of UMZC T1041 comes very close to that of

483   a pleurodiran processus trochlearis pterygoidei. Additionally, although the external process of

484   the pterygoid is anteriorly sutured to the jugular-maxillar area in many turtles, including some

485   cryptodires (chelydrids) and early stem turtles like *Proganochelys quenstedtii* (e.g. Gaffney,

486   1990), the deep and large facet for the articulation with the jugal (Fig. 6B–C, 4) demonstrates an

487   unusually strong structural integration of the external process into the mechanical framework of

488   the cranium, as is also seen in pleurodires. However, the lateral surface of the external process is

489   parallel to the sagittal skull plane (Fig. 2B), and the process is not laterally tilted with its

490   posterior end, as is the case in pleurodiran pterygoid trochleae. As such, the trajectory of the

491   adductor muscles, when approximated around the weak otic trochlea present on the prootic of

492   UMZC T1041, do not seem to be guided around the external process, implying functional

493   differences in the structure described for *Pleursternon bullockii* and the processus trochlearis

494   pterygoidei of pleurodires. As the detailed morphology of the external process is rarely described

495   in detail, we cannot exclude the possibility that this morphology is perhaps wider spread that

496   noted herein.

497   The dorsal surface of the pterygoid of UMZC T1041 is curved around the anteriorly

498   narrowing parabasisphenoid. Posteriorly, the medial part of the dorsal surface is dominated by a

499   low buttress for articulation with the prootic and parabasisphenoid, which also forms the medial

500   wall of the canalis cavernosus (Fig. 6B–C). The lateral surface of this canal is formed by the

501   crista pterygoidei. The canalis cavernosus ends anteriorly in the foramen cavernosum formed

502 between the prootic and pterygoid. Anterior to the foramen, the canalis cavernosus continues as

503 the sulcus cavernosus and parallels the rostrum basisphenoidale of the parabasisphenoid (Fig.

504 6B–C). At the anterior end of the crista pterygoidei, there is a small exiting foramen for the

505 canalis nervus vidianus (Evans & Kemp, 1975; Fig. 6B–C). The crista pterygoidei itself is

506 relatively low and posteriorly interrupted by a deep notch for the trigeminal foramen. In the

507 posterior margin of this foramen, the pterygoid extends dorsally to reach the parietal and thus

508 excludes the prootic from contributing to the foramen (Fig. 4B). The same dorsal process is

509 present in *Uluops uluops* (UCM 53971). The crista pterygoidei of UMZC T1041 is laterally

510 overlapped by the epipterygoid anterior to the trigeminal foramen (Fig. 4B).

511

512 **Supraoccipital.** The supraoccipital of UMZC T1041 is nearly completely preserved. It

513 ventrolaterally contacts the prootic and opisthotic and perhaps has a point contact with the

514 quadrate (Figs. 2, 4). It furthermore contacts the parietal anteroventrally and dorsally, and likely

515 contacted the exoccipital posteroventrally.

516 The supraoccipital of UMZC T1041 forms a comparatively broadly arched roof to the

517 endocranial cavity (Fig. 2F). A vertical plate extends over the entire anteroposterior length of the

518 supraoccipital, but this plate does not seem to extend posteriorly from the approximate position

519 of the foramen magnum as a supraoccipital crest (Evans & Kemp, 1975). This crest seems

520 dorsally nearly completely covered by the parietals. The supraoccipital was likely only

521 marginally visible in the skull roof between the parietals, though much less than interpreted by

522 Evans & Kemp (1975). This differs from the conditions in *Uluops uluops* (UCM 53971),

523 *Glyptops ornatus* (Gaffney, 1979a), and *Dorsetochelys typocardium* (Evans & Kemp, 1976), in

524 which the supraoccipital crest is topped by a triangular or diamond shaped horizontal plate that

525   forms a marginal part of the dorsal skull roof. Within the otic capsule of UMZC T1041, the

526   supraoccipital articulates with the prootic anteriorly and the opisthotic posteriorly. Between both

527   bones, the supraoccipital likely extends laterally to have a small superficial contact with the

528   quadrate, as is also the case in *Uluops uluops* (UCM 53971). The hiatus acusticus of UMZC

529   T1041 is a large, unossified space between the supraoccipital, prootic, parabasisphenoid, and

530   opisthotic, leaving a large opening between the inner ear cavity and the endocranial cavity.

531   Dorsally above the hiatus acusticus, the foramen aquaducti vestibuli, i.e. the canal for the

532   endolymphatic duct, is completely embedded within bone, forming a short canal from the

533   endocranial cavity into the recess of the supraoccipital that holds the common crus of the

534   labyrinth. Evans & Kemp (1975) reported that the foramen aquaducti vestibuli is only a notch in

535   the supraoccipital margin, but as completely ossified canals exist on both sides of the

536   supraoccipital, they probably misinterpreted a small break on the left side of the element and

537   missed the small foramina. Contacts with the lost exoccipitals can be inferred from short facets

538   posterior to the articulation site for the opisthotic.

539

540   **Exoccipital.** The exoccipitals are not preserved in UMZC T1041.

541

542   **Basioccipital.** The basioccipital is not preserved in UMZC T1041.

543

544   **Prootic.** Both prootics of UMZC T1041 are present, but the right one is better preserved. The

545   prootic has a large exposure within the floor of the adductor chamber, forming the anteromedial

546   part of the otic capsule (Fig. 4). Its dorsal surface is transversely concave and anteroventrally

547   sloping toward the subtemporal fossa (Fig. 4A). Although this surface does not protrude

548   anteriorly into the fossa, this morphology clearly indicates a redirecting of the jaw adductor

549   musculature. Thus, a small processus trochlearis oticum is present. A very similar morphology,

550   although more pronounced by a deeper concave flexure across the prootic, is seen in *Uluops*

551   *uluops* (UCM 53971). Anteroventrally, the prootic of UMZC T1041 forms the dorsal margin of

552   the foramen cavernosus. Slightly anterodorsally to the position of this foramen, the prootic is

553   slightly expanded transversely to form the posterior wall of the fossa epiptericum for the

554   trigeminal ganglion. However, the anteroventral margin of the prootic is excluded from the

555   trigeminal foramen itself, contra the description of Evans & Kemp (1975; Fig. 4B).

556   Medioventrally, the prootic has a large, foot-like process that contacts the pterygoid and

557   parabasisphenoid. The medial surface of this ventral prootic process is recessed by the fossa

558   acustico-facialis, from which the facial nerve canal extends through the ventral prootic process

559   toward the canalis cavernosus, and from which the short acustic nerve canals lead into the

560   prootic part of the cavum labyrinthicum. This cavity for the labyrinth deeply excavates the

561   prootic from posterior (Fig. 5A–B). The canal for the lateral semicircular duct of the labyrinth

562   organ is already ossified within the prootic, and thus shared between prootic and opisthotic (Fig.

563   5B, D). Ventrally, a horizontal footplate of the ventral prootic process extends posteriorly and

564   floors the anterior half of the cavum labyrinthicum (Fig. 5). This footplate contacts the opisthotic

565   across the entire transverse width of the cavum labyrinthicum, so that the fenestra ovalis is

566   completely surrounded, dorsally and ventrally, by these two bones (Fig. 5C–D). The same

567   condition is present in *Uluops uluops* (UCM 53971) and *Glyptops ornatus* (Gaffney, 1979a).

568   Laterally to the fenestra ovalis of UMZC T1041, and thus within the cavum acustico-jugulare,

569   the posteriorly exposed surface of the prootic is deeply recessed by a fossa (Fig. 5B–C), which

570   has been hypothesized to be related to the perilymphatic system of reentrant fluid-flow systems

571   in turtle ears (e.g. Evers & Benson, 2019; Evers et al., 2019; Foth et al., 2019), and which is also

572   present in *Uluops uluops* (UCM 53971). Because the fossa continues dorsolateral to the fenestra

573   ovalis onto the opisthotic, we use the term perilymphatic fossa instead of posterior prootic recess

574   as in some previous works (e.g. Evers & Joyce, 2020). Laterally to the perilymphatic fossa, the

575   pterygoid and prootic form the posterior foramen for the canalis cavernosus. The mediodorsal

576   wall of the canalis cavernosus, formed by the prootic, is incised by a sulcus for the

577   hyomandibular nerve (Fig. 5B), which extends from the lateral foramen of the facial nerve canal

578   to the posterior foramen for the canalis cavernosus. Such a sulcus is also present in *Uluops*

579   *uluops* (UCM 53971).

580

581   **Opisthotic.** The opisthotics are nearly completely preserved on both sides of the cranium of

582   UMZC T1041, but while the left one remains in articulation with the adjacent prootic and

583   quadrate on the left side, the right one is ventrally displaced (Figs. 2B, F, 5C–D). The opisthotic

584   contacts the prootic anteriorly, the supraoccipital medially, the exoccipital

585   posteroventromedially, the parabasisphenoid ventrally, the quadrate and squamosal laterally, and

586   the pterygoid ventrally.

587   The anterior part of the opisthotic forms parts of the cavum labyrinthicum (Fig. 5C–D). On

588   the right opisthotic, the processus interfenestralis, which walls the cavum labyrinthicum

589   posteriorly, is broken off (Fig. 5A). On the left element, the process is also damaged, but still

590   preserved in articulation with the underlying pterygoid (Fig. 5C–D). The processus

591   interfenestralis is delicate in UMZC T1041, but resembles the process of *Eilaenchelys*

592   *waldmanni* (NMS.G.2004.31.15) and more crownward positioned stem-turtles by reaching

593   ventrally to fully separate the cavum labyrinthicum from the recessus scalae tympani. At the

594   dorsal base of the processus interfenestralis, the lateral foramen for the glossopharyngeal nerve is

595   visible (Fig. 5A, C). The ventral end of the process is expanded to a small footplate that

596   articulates with the dorsal surface of the pterygoid, and frames the fenestra ovalis

597   posteroventrally (Fig. 5C–D). The footplate of the process also minimally contacts the

598   parabasisphenoid, which has a dorsally high margin surrounding the 'cup' that holds parts of the

599   brain. The processus interfenestralis is centrally broken on the left side of UMZC T1041,

600   probably where the fenestra perilymphatica minimized its structural integrity. Whereas the

601   ventral part with the footplate is in perfect articulation with the prootic and pterygoid, the dorsal

602   part of the process and the remainder of the left opisthotic are slightly misplaced with regard to

603   their original position. Although the fenestra perilymphatica is thus collapsed, there is no reason

604   to believe its size was smaller than that of other turtles, as sometimes stated for paracryptodires

605   and *Pleurosternon bullockii* specifically (e.g. Brinkman & Nicholls, 1993; Gaffney, 1996; Joyce,

606   2007). Additionally, the perilymphatic foramen of *Uluops uluops* (UCM 53971) is of 'regular'

607   size, and the morphology of the processus interfenestralis of this taxon is very similar to that of

608   *Pleurosternon bullockii*. Laterally and slightly anteriorly to the base of the processus

609   interfenestralis of UMZC T1041, there is a shallow sulcus in the roof of the cavum acustico-

610   jugulare, the perilymphatic fossa, which continues anteriorly to become confluent with

611   respective fossa on the prootic (Fig. 5C). The presence of this sulcus, its connection to the

612   prootic fossa, and its posterior end at the base of the processus interfenestralis, and thus near the

613   recessus scalae tympani, provide further tentative evidence that the fossa indeed is associated to

614   the soft tissues that form an enclosed fluid-flow system between the fenestra ovalis, cavum

615   labyrinthicum, foramen perilymphatica, and recessus scalae tympani (e.g. Evers & Benson,

616   2019; Foth et al., 2019).

617   A large facet for the exoccipital spans over the posteromedial margin of the opisthotic (Fig.

618   5A). The facet extends posteriorly halfway along the paroccipital process, indicating that the

619   exoccipital had an elongate posterodorsolateral process. The size of the exoccipitals as inferred

620   from their opisthotic facets suggests that the recessus scalae tympani, which is posteriorly framed

621   by the exoccipital, was a large element. The dorsal margin of the foramen jugulare anterius is

622   visible as a gentle notch in the opisthotic's margin with the brain cavity (Fig. 5A) and located

623   just anterior to the facet for the exoccipital.

624   The paroccipital process of the opisthotic is relatively flat dorsoventrally (Figs. 2F, 5A), as in

625   *Uluops uluops* (UCM 53971), and has a thin edge posterior to the articulation facet for the

626   exoccipital. The lateral surface of the process lies against the quadrate and both are dorsally

627   overlapped by the squamosal.

628

629   **Parabasisphenoid.** The parabasisphenoid of turtles develops from the fusion of the

630   parasphenoid and basisphenoid (Sterli et al., 2010). Although some regin of the fused

631   parabasisphenoid can be attributed relatively safely to the original ossification centers, as

632   hypothesized by Sterli et al. (2010) for several taxa including *Pleurosternon bullockii*, the CT

633   scan of UMZC T1041 gives no indication as to where the suture between both ossifications lies.

634   Thus, the basisphenoid and parasphenoid are completely fused in UMZC T1041. In

635   consequence, we segmented the parabasisphenoid as a single element, and describe it as such

636   without distinguishing the parasphenoid and basisphenoid regions. The parabasisphenoid of

637   UMZC T1041 is completely preserved and contacts the pterygoid, prootic, opisthotic, and

638   basioccipital (Figs. 2B, 7). A contact with the exoccipital is not preserved, but cannot be ruled

639   out, as well as possible anterior contacts with the palatines or the vomer. The parabasisphenoid

640   of *Pleurosternon bullockii* is anteroposteriorly elongate and mediolaterally narrow (Fig. 7). The

641   ventrally exposed surface of the parabasisphenoid is vaguely triangular, as the parabasisphenoid

642   narrows anteriorly to the rostrum basisphenoidale. Although the pterygoids are not in perfect

643   articulation with the parabasisphenoid in UMZC T1041, it seems that the ventral surface of the

644   rostrum basisphenoidale was exposed ventrally, separating the pterygoids and preventing them

645   from having a midline contact (see also Evans & Kemp, 1975). Indication for this interpretation

646   comes from anteroposterior grooves to either side of the rostrum basisphenoidale (Fig. 7B),

647   which we interpret to be the articular facets of the pterygoid. The ventral surface of the

648   parabasisphenoid between these facets is completely smooth, just as the adjacent ventral surface

649   of the pterygoids, further support the notion that this bone was exposed. Conversely, parts of the

650   parabasisphenoid that are overlapped by the pterygoid are usually roughened by articular ridges

651   in comparative taxa like *Uluops uluops* (UCM 53971). A ventrally exposed rostrum

652   basisphenoidale has also been described for *Glyptops ornatus* (Gaffney, 1979a), but it remains

653   unclear, though plausible, if the pterygoids are fully separated by the parabasisphenoid in both

654   taxa.

655   At about half the length of the parabasisphenoid of UMZC T1041, the basipterygoid process

656   projects laterally from the ventrolateral margin of the bone (Fig. 7B–C, E). Although it has been

657   argued that the process on the lateral margin of the basisphenoid of UMZC T1041 does not

658   constitute a basipterygoid process (Gaffney, 1979a; Sterli et al., 2010), we agree with the original

659   identification of Evans & Kemp (1975) and later assessments of the structure (e.g., Rabi et al.,

660   2013). The basipterygoid process is subdivided into a dorsal and a ventral flange by a deep

661   sulcus for the cerebral artery (Fig. 7E), which is also the case in *Uluops uluops* (UCM 53971).

662   The dorsal flange is likely homologous with the basipterygoid process of other turtles, as the

663   carotid system extends ventrally to it. The cerebral artery canal of UMZC T1041 fully enters the

664   parabasisphenoid just anterior to the basipterygoid process via the foramen posterius canalis

665   carotici cerebralis (see also Sterli et al., 2010) and projects anteromedially through the bone (Fig.

666   7E). The dorsal flange of the basipterygoid process is larger, and inserts deeply into the

667   respective facet on the pterygoid. Anterior to the foramen posterius canalis carotici cerebralis,

668   there is a faint and narrow groove that extends along the ventrolateral surface of the rostrum

669   basisphenoidale. This groove is herein not interpreted as a narrow canal for the palatine artery, as

670   it is not mirrored in the pterygoid bone. Instead, the pterygoid would fill the groove when

671   articulated tightly with the parabasisphenoid. Thus, we herein interpret the groove as the

672   delimitation of the facet for the pterygoid (Fig. 7B, E). The palatine canal therefore appears to be

673   absent in UMZC T1041.

674   A peculiar feature of the basicranium of UMZC T1041 is the presence of a posterior process

675   jointly formed by the parabasisphenoid and pterygoid (Fig. 7B–C, E), which overlaps the ventral

676   surface of the basioccipital. The parabasisphenoid part of this process is larger and more distinct

677   than the pterygoid part. In UMZC T1041, the ventral surface of the posterior parabasisphenoid

678   processes is slightly raised, and forms a shallowly concave fossa between them. Additionally, the

679   surface of the process is textured by a short ridge. Such parabasisphenoid processes are also

680   present in *Glyptops ornatus* (Gaffney, 1979a) and *Uluops uluops* (UCM 53971), and could be a

681   pleurosternid synapomorphy. Posterolaterally projecting processes of the parabasisphenoid are

682   also present in some baenids, such as *Eubaena cephalica* (Rollot, Lyson & Joyce, 2018), but the

683   baenid process has less external relief, and seems better integrated into a flat ventral surface of

684   the basicranium. Similar structures are also found in helochelydrids, in which these are

685   sometimes referred to as a secondarily pair of tubercula basioccipitale (Joyce, Sterli & Chapman,

686   2014). In helochelydrids, these anterior tubercula basioccipitale are predominantly formed by the

687   pterygoids (*Naomichelys speciosa*: Joyce, Sterli & Chapman, 2014), or entirely formed by the

688   pterygoids (*Helochelydra nopscai*: Joyce et al., 2011). Despite these differences in composition

689   of the processes, the anterior tubercula basioccipitale of helochelydrids and the posterior

690   parabasisphenoid processes of pleurosternids share (i) that the posterior margin between them is

691   concave; (ii) that they are slightly raised and form a concavity medially between them; (iii) that

692   they overlap the basioccipital; and (iv) that their surface is textured indicating soft tissue

693   insertion. Thus, topological and anatomical arguments suggest the homology of the pleurosternid

694   and helochelydrid processes, and possibly provide evidence for paracryptodiran affinities of

695   helochelydrids (see also Joyce, 2017; Joyce & Anquetin, 2019). To highlight this possible

696   homology, we follow Joyce, Sterli & Chapman (2014) by calling these processes (anterior)

697   tubercula basioccipitale (Fig. 7).

698   The dorsal surface of the parabasisphenoid of UMZC T1041 is extremely similar to the same

699   surface in *Uluops uluops* (UCM 53971) and YPM 4717, a specimen referred to *Glyptops*

700   *plicatulus* by Gaffney (1979a) (*Glyptops ornatus* according to taxonomy followed here) based on

701   temporal and geographic reasoning. It can be divided into a posterior, slightly cup-like region

702   that holds parts of the brain, and the rostrum basisphenoidale anteriorly (Fig. 7A). In the

703   posterior region, the parabasisphenoid is dorsoventrally thickest. The posterolateral margin of the

704   parabasisphenoid is dorsally expanded. This expansion, which is also present in *Uluops uluops*

705   (UCM 53971), forms the ventral margin of the hiatus acusticus (Fig. 7A) and contacts the

706   processus interfenestralis of the opisthotic posteriorly and the prootic anteriorly (Fig. 5D). The

707   lateral margins of the parabasisphenoid anterior to the hiatus acusticus margin are gently raised,

708   so that the medial space between is transversely concave (Fig. 7A). The concavity is interrupted

709 posteriorly by a shallow basis tuberculi basalis (Fig. 7A, D), which would presumably have

710 continued posteriorly onto the basioccipital, as seen in *Uluops uluops* (UCM 53971). Foramina

711 for the abducens nerve are present anterolaterally on the dorsal parabasisphenoid surface. The

712 respective anterior foramina exit on the anterior basisphenoid surface within the retractor bulbi

713 pits ventral to the clinoid processes. The clinoid processes at the anterolateral corner of the

714 parabasisphenoid cup are extremely short (Fig. 7A, D), as is also the case in *Uluops uluops*

715 (UCM 53971). The dorsum sellae between the clinoid processes of UMZC T1041 is not

716 developed as a vertical wall, but also not as a horizontal sheet that overlaps the sella turcica.

717 Instead, the dorsum sellae is only a very minor, shallow ridge (Evans & Kemp, 1975; Fig. 7D).

718 Ventrally underneath the ridge, the anterior surface of the parabasisphenoid slopes toward the

719 rostrum basisphenoidale and sella turcica. This anterior surface is gently depressed and a midline

720 ridge is absent (Fig. 7D). The lateral aspects of the anterior surface are delimited by short vertical

721 ridges that extend from the base of the clinoid process downwards. These ridges also define deep

722 retractor bulbi pits directly ventral to the clinoid processes (Fig. 7D). The retractor bulbi pits are

723 further accentuated dorsally by a horizontal ridge at the base of the clinoid process, which is the

724 same in *Glyptops ornatus* (Gaffney, 1979a). In *Uluops uluops* (UCM 53971), the anterior surface

725 of the parabasisphenoid varies from *Glyptops ornatus* and *Pleurosternon bullockii* in lacking

726 distinct retractor bulbi pits and having a deeper anterior surface ventral to the dorsum sellae. The

727 rostrum basisphenoidale of UMZC T1041 extends anteriorly as a mediolaterally narrow sheet of

728 bone. Its lateral margins are dorsally upturned, so that the sella turcica is well defined as a deep

729 fossa (Fig. 7A, D). In the posterior margin of the sella turcica, the paired foramina anterius

730 canalis carotici cerebralis are situated in relatively close proximity to one another (Fig. 7D).

731

732   **Stapes.** The stapes are not preserved for UMZC T1041.

733

734   **Carotid circulation and facial nerve.** Unambiguous osteological correlates are present in

735   UMZC T1041 for the cerebral artery, the (undivided) facial nerve, and both major distal

736   branches of the facial nerve, which are the hyomandibular and vidian nerves. As there is no

737   evidence for a palatine artery canal, the palatine artery is either absent, or uncovered by bone, but

738   located in an unusual position.

739   As described above (see parabasisphenoid), the basipterygoid process of UMZC T1041 is

740   subdivided into a dorsal and a ventral flange (Fig. 7B–C, E), between which the canal for the

741   cerebral artery starts to pierce the parabasisphenoid (Fig. 7E). This region is ventrally exposed,

742   as the parabasisphenoid and pterygoid form a window-like recess around the basipterygoid

743   articulation. No canalis caroticus internus is present posterior to the position of the basipterygoid

744   process, so that the internal carotid artery is not embedded in bone (see also Sterli et al., 2010).

745   As the ventral flange of the basipterygoid process is much smaller than the dorsal flange, the

746   artery can enter the basicranium via the small fenestra between the pterygoid and

747   parabasisphenoid. As the artery directly enters the parabasisphenoid in this position, we do not

748   classify this opening within the basipterygoid articulation as a foramen posterius canalis carotici

749   interni (as done in Evans & Kemp, 1975), but as the foramen posterius canalis carotici cerebralis

750   (as in Sterli, 2010). The palatine artery canal, if present, would be expected to extend anteriorly

751   between the pterygoid and parabasisphenoid from the position of the foramen posterius canalis

752   carotici cerebralis. Gaffney (1979a) indicated the presence of such a canal for *Glyptops ornatus*,

753   but this should be revisited, as he did not find the anterior foramen for the palatine artery canal

754   and thus might have misidentified the foramen for the vidian canal. In UMZC T1041, no palatine

755   artery canal can be discerned. The parabasisphenoid, which is slightly disarticulated from the left

756   pterygoid and strongly so from the right one, shows a subtle and narrow groove, that extends

757   from the foramen posterius canalis carotici cerebralis forward and could thus be a candidate

758   structure for the palatine artery canal (Fig. 7B). However, when the pterygoid is articulated, the

759   respective groove is 'closed' by bone of the pterygoid, so that the groove likely constitutes a

760   pterygoid facet, rather than a tiny canalis caroticus palatinum. As the posterior course of the

761   internal carotid artery prior to its 'split' is not embedded in bone, the absence of the palatine

762   artery canal does not necessarily warrant concluding that the artery itself is absent. However, as

763   there is no indication of an interpterygoid slit or similar opening through which the palatine

764   artery could eventually enter the cranium in UMZC T1041 or related taxa with more completely

765   preserved anterior palate regions, the most parsimonious explanation of the observed pattern

766   indeed is the loss of the palatine artery. The loss of the palatine artery has also been inferred for

767   other paracryptodires (Gaffney, 1975a; Lipka et al., 2006), including baenids (Rollot, Lyson &

768   Joyce, 2018). However, the absence does not seem universal, as *Uluops uluops* clearly shows a

769   palatine artery canal (UCM 53971). A palatine artery canal has also been reported for

770   *Dorsetochelys typocardium* by Anquetin and André (2020), but these authors do not describe the

771   canal system in detail and it thus remains unclear if the proposed palatine artery canal foramen

772   reported for *Dorsetochelys typocardium* is indeed that or pertains to the canal system of the

773   vidian nerve. Indeed, the posterior entry of the palatine artery described by Anquetin and André

774   (2020) resembles that of the vidian canal described herein for *Pleurosternon bullockii* by

775   piercing the pterygoid. As the situation in *Dorsetochelys typocardium* demands clarification,

776   ideally by means of CT scanning, we will not further comment on this taxon herein. The

777   condition of *Uluops uluops* (UCM 53971) is very similar to that *Pleurosternon bullockii* by

778   having the carotid canal enter within a bifurcated basipterygoid process, although the former also

779   has a foramen for the palatine artery. *Uluops uluops* (UCM 53971) shows, that no part of its

780   internal carotid artery up to the point of its division is embedded by bone. In *Arundelemys*

781   *dardeni*, the internal carotid artery itself is also not encased anteriorly, the palatine artery is

782   absent, and the entry of the cerebral artery canal lies within a shallow fossa between the

783   parabasisphenoid and pterygoid. All these turtles differ from baenids, in which the anterior part

784   of the internal carotid artery is concealed by bone. This embedding of the internal carotid artery

785   in baenids extends posteriorly up to the intersection of the carotid artery system with the canalis

786   pro ramo nervi vidiani (Rollot, Lyson & Joyce, 2018). On the other hand, similarities between

787   baenids, *Pleurosternon bullockii*, and *Arundelemys dardeni* exist in their shared absence of a

788   palatine artery. Thus, most paracryptodires show similarities to one another in their carotid artery

789   system, but lots of within-group variation exists that can probably only be better understood once

790   the phylogenetic relations of these turtles are better characterized.

791   The facial nerve of UMZC T1041 exits the braincase laterally through the canalis nervus

792   facialis, which extends from the fossa acustico-facialis through the prootic and into the canalis

793   cavernosus. The position of the geniculate ganglion can be inferred to be within the canalis

794   cavernosus for UMZC T1041, because direct osteological evidence for the course of the

795   hyomandibular and vidian nerves begin there: the prootic has a hyomandibular sulcus that

796   extends from the lateral facial nerve canal foramen posteriorly to the cavum acustico-jugulare

797   (Fig. 7B). The vidian nerve passes ventrally through the pterygoid via the canalis pro ramo nervi

798   vidiani, which exits just posterior to the pterygoid ridge that borders the area of the basipterygoid

799   articulation (Fig. 7C). In turtles with an embedding of the internal carotid artery, the canalis pro

800   ramo nervi vidiani usually leads from the canalis cavernosus into the internal carotid canal (e.g.

801   Gaffney, 1979b). In UMZC T1041, which lacks an internal carotid canal, the vidian nerve is thus

802   transmitted to the ventral surface of the basicranium. From here, it is inferred to pass between the

803   dorsal and ventral flanges of the basipterygoid process, together with the carotid artery. Within

804   the facet for the basipterygoid process, the vidian nerve then enters the canalis nervus vidianus,

805   which starts in the center of the facet and extends anteriorly through the pterygoid. This posterior

806   foramen for the vidian canal was interpreted as a foramen posterius canalis carotici palatinum by

807   Sterli et al. (2010). However, the canal extends through the pterygoid only, instead of passing

808   along the parabasisphenoid-pterygoid suture, and exits anterolaterally from the sulcus cavernosus

809   (Fig. 6B, C), instead within the sulcus itself. Thus, the course and exit foramen of the canal

810   conform to the expectations of a canalis nervus vidianus (Rollot, Lyson & Joyce, 2018).

811

812   **DISCUSSION**

813   **Paracryptodiran monophyly.** The fossil turtle clade Paracryptodira was initially proposed

814   based on the anterior position of the foramen posterius canalis carotici interni halfway along the

815   contact of the basisphenoid with the pterygoid, in contrast to pleurodires, which have an entry

816   that involved the prootic and/or quadrate, and crown cryptodires, which have an entry towards

817   the posterior margin of the pterygoid (Gaffney, 1975a). The accuracy and utility of this character

818   has been debated ever since (e.g., Evans & Kemp, 1976; Gaffney, 1979a; Rieppel, 1980; Sterli et

819   al., 2010; Rabi et al., 2013), but progress has been hampered by confusing terminology and

820   conflicting observations.

821   Our study suggests that two distinct morphotypes are present among paracryptodires.

822   Whereas an anteriorly positioned foramen posterius canalis carotici interni indeed seems to be

823   present in *Compsemys victa* (UCM 53971) and *Eubaena cephalica* (Rollot, Lyson & Joyce,

824   2018), this foramen is not present in *Pleurosternon bullockii* (UMZC T1041) and *Uluops uluops*

825   (UCM 53971), as the internal carotid artery is embedded in bone in these taxa. This difference

826   was initially disguised by terminology used from the 1970s to early 2000s, as the foramen

827   posterius canalis carotici cerebralis was addressed as the foramen posterius canalis carotici

828   interni (Rabi et al., 2013). Homology can nevertheless be maintained, if the foramen posterius

829   canalis carotici interni is conceptualized as the entry to a small pit at the basisphenoid/pterygoid

830   suture from which the cerebral and palatine arteries penetrate the surrounding bones, as had been

831   reported for several paracryptodires, including *Glyptops ornatus* (Gaffney, 1979) or

832   *Pleurosternon bullockii* (Sterli et al., 2010), but we are here able to demonstrate that this

833   character concept is at least inapplicable to the latter, as the palatal canal is absent.

834   The above-listed differences should not be used to dismiss the fact that the carotid system, in

835   general, enters the skull in all known paracryptodires from below relatively far anteriorly at or

836   near the basisphenoid/pterygoid suture. Indeed, as the exact vessels penetrating the skull could

837   only rarely be assessed prior to the use of CT scanning technology, we suspect from personal

838   experience (WGJ) that the paracryptodiran condition was conceptualized by most authors by

839   reference to topology, not the exact vessels that enter the skull. This broadened character

840   concept, however, still pertains to two unrelated morphological aspects: first, the anterior

841   placement of the entry of the carotid system and, second, the presence of an extended

842   basisphenoid-pterygoid contact. The (derived) presence and extent of the basisphenoid-pterygoid

843   contact is addressed in current phylogenetic analyses by other characters (e.g. Joyce, 2007;

844   Sterli, 2010; Anquetin, 2012; Zhou & Rabi, 2015; Evers & Benson, 2019), while the

845   (plesiomorphic) anterior placement of the carotid system entry could be grouped with the

846   condition seen in basal turtles. So, while these two morphological aspects combined indeed

847   diagnose paracryptodires relative to most other turtles, they are redundant with existing

848   characters. We therefore here further support recent phylogenetic analysis (e.g. Evers & Benson,

849   2019) by suggesting that the 'paracryptodiran condition' should not be utilized as a carotid

850   arterial character.

851   Although the most important 'paracryptodiran' cranial character can thus be debunked,

852   pleurosternids, baenids, and other potential paracryptodires share several features that could

853   potentially support their monophyly. In addition to the sculpturing of the shell (present in early

854   baenids; e.g. Gaffney, 1972; Joyce & Anquetin, 2019), baenids and pleurosternids share some

855   gross resemblance in their maxilla-premaxilla morphology, including a relatively strongly curved

856   labial margin of the maxilla and a notch in the median section of the labial ridge along the

857   premaxilla (Gaffney, 1972). Additionally, the jugal is dorsally removed from posteriorly

858   continuing the labial ridge otherwise formed by the maxilla (Gaffney, 1972). These features are,

859   however, not unique to paracryptodires, as they also appear in extant turtles with ecologies that

860   are probably similar to those of paracryptodires, such as riverine geoemydids (e.g. Gaffney,

861   1979b). To critically assess potential new paracryptodiran synapomorphies, the skulls of early

862   baenids, particularly *Trinitichelys hiatti*, should be re-described.

863

864   **Paracryptodiran relationships.** This contribution is part of a larger study that attempts to better

865   resolve the internal and external relationships of paracryptodires, if monophyletic, through a

866   better understanding of their anatomy. Although the novel observations we made herein will be

867   processed in later contributions, we take the liberty of highlighting similarities that particularly

868   intrigue us and that may have phylogenetic significance.

869   Irrespective of paracryptodiran monophyly, our description of *Pleurosternon bullockii*

870   provides morphological evidence for the content of Pleurosternidae, based on instances of

871   similarities of *Pleurosternon bullockii* with some other taxa. Although a re-description of

872   *Glyptops ornatus* is warranted to fully appreciate its anatomy, it is clear from existing

873   information (e.g. Gaffney 1979a) that this taxon is indeed very similar to *Pleurosternon*

874   *bullockii*, both in terms of general skull form, and in more detailed anatomical aspects. For

875   instance, *Pleurosternon bullockii* and *Glyptops ornatus* share the following features: small

876   prefrontals; long anterior processes of the frontals that partially separated the nasals; a

877   squamosal-parietal contact; dorsal position of the jugal above the level of the labial margin of the

878   maxilla; and, among other similarities in the parabasisphenoid morphology, the presence of

879   anterior tubercula basioccipitale, the presence of a basipterygoid process, and the presence of

880   deep retractor bulbi pits. The same is generally true for *Dorsetochelys typocardium*, in particular

881   the jugal exclusion from the orbit (DORCM G.00023; *contra* Evans & Kemp 1976) and the

882   presence of anterior tubercula basioccipitale (DORCM G.00023; not discernible in Evans &

883   Kemp 1976). In both cases, these similarities are not surprising, given that more recent

884   phylogenetic hypotheses already highlight close relationships among these turtles (e.g. Pérez-

885   García, Royo-Torres & Cobos, 2015; Joyce & Rollot, in press).

886   Although the skull of *Uluops uluops* deviates in general aspects of its cranial shape, we note a

887   great number of similarities between this taxon and *Pleurosternon bullockii*. Although *Uluops*

888   *uluops* has so far not been considered a pleurosternid (e.g. Carpenter & Bakker, 1990; Lyson &

889   Joyce 2011, Pérez-García, Royo-Torres & Cobos, 2015; Joyce and Rollot, in press), our

890   comparisons indicate that it might be attributable to this clade. Among the features that are

891   shared between *Uluops uluops* and *Pleurosternon bullockii* are a squamosal-parietal contact

892   (possibly plesiomorphically present in baenids; Gaffney 1972); the exclusion of the prootic from

893   the trigeminal foramen by a posteroventral ramus of the parietal (also present in

894   thalassochelydians and sandownids; Anquetin, Püntener & Joyce, 2017; Evers & Joyce, 2020);

895   the presence of an extended sulcus palatino-pterygoideus formed in part by an enlarged septum

896   orbitotemporale (similar to pleurodires, but also present in some cryptodires; Gaffney, Tong &

897   Meylan, 2006); presence of a deep fossa in the roof of the sulcus palatino-pterygoideus (also in

898   pleurodires; Gaffney, Tong & Meylan, 2006); dorsal position of the jugal above the level of the

899   labial margin of the maxilla (also present in baenids; Gaffney 1972); the size and shape of the

900   quadratojugal; the presence of a small quadrate-supraoccipital contact (unclear in early baenids);

901   the complete surrounding of the fenestra ovalis by the prootic and opisthotic (absent in

902   *Arundelemys dardeni* [USNM 41614]; unclear in other early baenids); the presence of a

903   hyomandibular nerve sulcus in the posterior part of the canalis cavernosus (unclear in early

904   baenids); the presence of anterior tubercula basioccipitale (shared also with helochelydrids, see

905   below); the presence of a basipterygoid process that is laterally invaded by the cerebral artery

906   (absent in baenids and *Compsemys victa*, but symplesiomorphic for turtles); and the general

907   shape of the parabasisphenoid (see description for full details). Although some of these

908   characters may prove to be more widespread among paracryptodires in particular or stem-turtles

909   more generally, the number of similar features between *Pleurosternon bullockii* and *Uluops*

910   *uluops* lend support to the hypothesis that the latter is a pleurosternid.

911   We here also document intriguing similarities between *Pleurosternon bullockii* and

912   helochelydrids, particularly in the anterior tubercula basioccipitale of the parabasisphenoid, but

913   also in other features, such as the exclusion of the jugal from the orbit (e.g. Joyce et al., 2011;

914   Joyce, Sterli & Chapman, 2014; Joyce 2017). Helochelydrids should be integrated into

915   phylogenies with a dense sampling of paracryptodires to test if they are more closely related than

916   currently thought.

917   We also note the presence of some features in *Pleurosternon bullockii* that are possibly more

918   widespread among crownward stem-turtles than previously recognized, and which can therefore

919   possibly aid in better constraining the global position of pleurosternids. For instance, a

920   pterygoid-basioccipital contact has previously not universally been recognized in pleurosternids

921   (but see Gaffney, 1979a). This feature, considered diagnostic for baenids (Joyce & Lyson, 2015),

922   is present in *Pleurosternon bullockii* and *Uluops uluops* (as well as in compsemydids and

923   helochelydrids). Although thus probably widely present among paracryptodires, this feature

924   probably cannot serve as a paracryptodiran synapomorphy, as several other clades that have

925   repeatedly been hypothesized to be crownward stem turtles (e.g. Joyce 2007), including

926   thalassochelydians, protostegids, and some xinjiangchelyids, also possess a pterygoid-

927   basioccipital contact (Brinkman et al., 2013; Anquetin, Püntener & Joyce, 2017; Evers, Barrett &

928   Benson, 2019). Conversely, we here demonstrate that a purported thalassochelydian

929   synapomorphy, the presence of a posteroventral process of the parietal along the posterior

930   margin of the trigeminal foramen (Anquetin, Püntener & Joyce, 2017), is also present in

931   *Pleurosternon bullockii* (and also *Uluops uluops*). The two examples of the pterygoid-

932   basioccipital contact and the presence of a posteroventral parietal process are a nice

933   demonstration of how alleged synapomorphies or diagnostic features of relatively inclusive

934   groups can have a much wider distribution across phylogeny. This highlights (i) the importance

935   of detailed descriptive work to acknowledge the anatomical variation present across several

936   clades; and (ii) the importance of global phylogenetic approaches to the classification of fossil-

937   only turtle clades. The latter is because the character state distribution outside the 'focal clade'

938   has importance not only for inference of global phylogenetic placements, but also has an effect

939   on in-group relationships and the optimization and polarity of characters (e.g. Kluge & Farris,

940   1969; Farris, 1972; Nixon & Carpenter, 1993). The distribution of the pterygoid-basioccipital

941   contact, for instance, indicates that rather than being a local baenid synapomorphy, it possibly

942   represents a synapomorphy of the clade that includes paracryptodires but also other probable

943   crownward stem-turtle clades (e.g. Evers & Benson, 2019) such as xinjiangchelyids or

944   thalassochelydians. On the other hand, studies focused on more inclusive focal groups without a

945   global phylogenetic perspective often sample characters that document variation among the

946   suspected clade members to a finer level of detail than done in most global studies (e.g. Joyce &

947   Lyson, 2011, for paracryptodires). We think that it is important to reconcile the finer-level

948   studies with global phylogenetic approaches to address questions such as: do baenids and

949   paracryptodires form a monophylum?; or what is the global position of these clades? We hope

950   that detailed anatomical studies such as the one presented here lead to the recognition of new

951   phylogenetic characters as well as the revision of those that have been used in the past, so that

952   the outlined questions can be more comprehensively addressed in the future.

953   On a final note, we find that *Pleurosternon bullockii* shows some remarkable similarities with

954   pleurodire turtles, particularly in the orbitotemporal region of the skull, as well as the external

955   process of the pterygoid. However, the orbitotemporal region of most fossil turtles is not

956   sufficiently described to draw meaningful comparisons from the literature alone. CT scans of

957   several specimens available to us, such as the xinjiangchelyid *Annemys* sp. (IVPP V18106;

958   specimen described in Brinkman et al. [2013]), the probable sandownid *Solnhofia parsonsi* (TM

959   4023; specimen described in Gaffney [1975b]) or the plesiochelyid *Plesiochelys planiceps*

960   (OUMNH J1582; specimen described in Gaffney [1976]) show that a strong ventral ridge of the

961 postorbital that would form the septum orbitotemporale and define a narrow sulcus palatino-

962 pterygoideus is absent in these turtles. This indicates that the similarity observed between

963 *Pleurosternon bullockii* and pleurodires in regard to the septum interorbitale and related sulcus

964 palatino-pterygoideus is unique, and not more widespread across the turtle stem. Similarly, the

965 pleurodire-reminiscent morphology of the external pterygoid process of *Pleurosternon bullockii*

966 is not seen in other crownward stem-turtles: the vertical flange of the external process of the

967 pterygoid of *Pleurosternon bullockii* is comparatively larger than that of plesiochelyids or

968 *Annemys* sp. Although both the size of the vertical flange and its slight medial deflection at the

969 dorsal margin in *Pleurosternon bullockii* establishes some similarity to the pterygoid trochlea of

970 pleurodires, important differences remain. For instance, the surface of the vertical flange of the

971 external pterygoid process is oriented parallel to the sagittal skull plane, and not posterolaterally

972 inclined. Unfortunately, the morphology of the pterygoid trochlea is unknown for stem-

973 pleurodires (De Lapparent de Broin, de la Fuente & Fernandez, 2007), but a gradual evolution of

974 the pterygoid adductor musculature system via a double-trochlea along the external pterygoid

975 process and the otic capsule has been proposed as a possible evolutionary scenario (e.g. Joyce,

976 2007). Although the presence of a double trochlea does not seem to provide biomechanical

977 advantages according to analytical studies (Ferreira et al., 2020), all hypotheses for the evolution

978 of the pleurodire trochlea invoke a size increase of the external pterygoid process and its lateral

979 surface as an initial step (e.g. Joyce, 2007; Joyce & Sterli, 2012; Ferreira et al., 2020). Although,

980 at this point in time, we do not hypothesize that pleurosternids are stem-pleurodires, the

981 similarities noted herein should be further explored by additional comparisons and phylogenetic

982 implementation.

983

CONLUSIONS

984 **CONCLUSIONS**

985 The cranial anatomy of *Pleurosternon bullockii* and comparative descriptions confirm high

986 levels of similarity with other hypothesized pleurosternids, such as *Glyptops ornatus* or

987 *Dorsetochelys typocardium*. Additionally, we note a large number of similarities between

988 *Pleurosternon bullockii* and *Uluops uluops*, which possibly is a pleurosternid as well. Among

989 other features, these taxa share a similar basipterygoid region, with the symplesiomorphic

990 retention of a basipterygoid process and a ventrally unimbedded internal carotid artery course,

991 shared with earlier diverging stem-turtles. These features, along with a relatively extensive dorsal

992 skull coverage and weakly developed otic trochleae, support the hypothesis that pleurosternids

993 are globally positioned among an extended stem-lineage of turtles. Our anatomical description of

994 *Pleurosternon bullockii* provides tentative evidence for close relationships between

995 pleurosternids and helochelydrids, which share unusual posterior processes of the

996 parabasisphenoid that form a second set of (anterior) tuberculae basioccipitale.

997 Although variation regarding the internal carotid region of the cranium exists among

998 pleurosternids, it is clear that the anterior position of the foramen posterius canalis carotici

999 interni, historically used as a synapomorphy to unite baenids and pleurosternids as

1000 Paracryptodira, is not present in pleurosternids, and results from misinterpretation of the

1001 respective anatomy. As other paracryptodiran cranial synapomorphies are also dubious, our

1002 observations challenge previous observations upon which traditional hypotheses regarding the

1003 systematics of paracryptodires were built. Although the monophyly of paracryptodires is thus

1004 currently not supported by evidence from cranial anatomy, CT documentation of early baenid

1005 cranial morphology is outstanding, and may provide such evidence in the future.

1006   *Pleurosternon bullockii* shows a surprising number of similarities with pleurodires, which are

1007   seen in the area between the otic and temporal fossae. The formation of a relatively narrow

1008   sulcus palatino-pterygoideus by an expanded septum orbitotemporale is unparalleled in other

1009   crownward stem-turtles such as xinjiangchelyids or thalassochelydians. An expanded external

1010   pterygoid process with a dorsomedially deflected vertical flange also approaches the pleurodiran

1011   morphology. Further investigations are necessary to test if this morphology could be a model for

1012   an ancestral pleurodiran pterygoid trochlea.

1013

1014   **INSTITUTIONAL ABBREVIATION**

1015   **DORCM**   Dorset County Museum, Dorchester, United Kingdom.

1016   **IVPP**   Institute of Vertebrate Paleontology and Paleoanthropology, Chinese Academy of

1017   Sciences, Beijing, People's Republic of China.

1018   **NMS**   National Museum of Scotland, Edinburgh, United Kingdom

1019   **OUMNH**   Oxford University Museum of Natural History, University of Oxford, Oxford,

1020   United Kingdom.

1021   **UCM**   Museum of Natural History, University of Colorado, Boulder, Colorado, USA.

1022   **UMZC**   Museum of Zoology, Cambridge University, Cambridge, United Kingdom.

1023   **USNM**   United States National Museum, Smithsonian Institution National Museum of

1024   Natural History, Washington, D.C., USA.

1025   **TM**   Teylers Museum, Haarlem, The Netherlands.

1026   **YPM**   Yale Peabody Museum of Natural History, New Haven, Connecticut, USA.

1027

1028   **ACKNOWLEDGEMENTS**

1029   We thank Roger Benson (University of Oxford) for scanning the cranium of UMZC T1041 in

1030   our stead. Keturah Smithson is thanked for maintaining the scanner at the Cambridge

1031   Biotomography Center and Jason Head (University of Cambridge) is acknowledged for

1032   permission to study the specimen. We also thank Gabriel Ferreira, Olivier Rieppel, and Julien

1033   Claude for three reviews that helped to improve a previous version of this manuscript, and we

1034   thank Fabien Knoll for the editorial oversight of our submission. Particular thanks to Gabriel

1035   Ferreira for spotting a segmentation mistake that would have been annoying if it had been

1036   published. The work is supported by a grant from the Swiss National Science Foundation (SNF

1037   200021_178780/1).

1038

1039   **REFERENCES**

1040   **Anquetin J. 2012.** Reassessment of the phylogenetic interrelationships of basal turtles

1041   (Testudinata). *Journal of Systematic Palaeontology* **10(1):**3–45.

1042   **Anquetin J, Püntener C, Billon-Bruyat J-P. 2015.** *Portlandemys gracilis* n. sp., a new coastal

1043   marine turtle from the Late Jurassic of Porrentruy (Switzerland) and a reconsideration of

1044   plesiochelyid cranial anatomy. *PLoS ONE* **10(5):**e0129193.

1045   **Anquetin J, André C. 2020.** The last surviving Thalassochelydia—a new turtle cranium from

1046   the Early Cretaceous of the Purbeck Group (Dorset, UK). *PaleorXiv*.

1047   doi:10.31233/osf.io/7pa5c.

1048   **Anquetin J, Püntener C, Joyce WG. 2017.** A review of the fossil record of turtles of the clade

1049   Thalassochelydia. *Bulletin of the Peabody Museum of Natural History* **58(2):**317–369.

1050   **Brinkman DB, Nicholls EL. 1993.** The skull of *Neurankylus eximius* (Testudines: Baenidae)

1051   and a reinterpretation of the relationships of this taxon. *Journal of Vertebrate Palaeontology*

1052   **13(3):**273–281.

1053   **Brinkman DB, Everth DA, Xu X, Clark JM, Wu X-C. 2013.** Turtles from the Jurassic

1054   Shishugou Formation of the Junggar Basin, People's Republic of China, with comments on

1055   the basicranial region of basal eucryptodires. In: Brinkman et al., eds. *Morphology and*

1056   *Evolution of Turtles*. Dordrecht: Springer Science+Buisness Media, 147–172.

1057   **Cadena EA, Parham JF. 2015.** Oldest known marine turtle? A new protostegid from the Lower

1058   Cretaceous of Colombia. *PaleoBios* **32:**1–42.

1059   **Carpenter K, Bakker RT. 1990.** A new latest Jurassic vertebrate fauna, from the highest levels

1060   of the Morrison Formation at Como Bluff, Wyoming. Part II. A new baenid turtle. *Hunteria*

1061   **2(6):**1–19.

1062   **De Lapparent de Broin F, de la Fuente MS, Fernandez MS. 2007.** *Notoemys laticentralis*

1063   (Chelonii, Pleurodira), Late Jurassic of Argentina: new examination of the anatomical

1064   structures and comparisons. *Revue de Paléobiologie* **26(1):**99–136.

1065   **Evans J, Kemp TS. 1975.** The cranial morphology of a new Lower Cretaceous turtle from

1066   Southern England. *Palaeontology* **18(1):**25–40.

1067   **Evans J, Kemp TS. 1976.** A new turtle skull from the Purbeckian of England and a note on the

1068   early dichotomies of cryptodire turtles. *Palaeontology*, 19**(2):**317–324.

1069   **Evers SW. 2020.** Project: Cranial CT scans of *Pleurosternon bullockii*. *MorphoSource*.

1070   Available at: https://www.morphosource.org/Detail/ProjectDetail/Show/project_id/1001

1071 **Evers SW, Benson RBJ. 2019.** A new phylogenetic hypothesis of turtles with implications for

1072 the timing and number of evolutionary transitions to marine lifestyles in the group.

1073 *Palaeontology* **62(1):**93–134.

1074 **Evers SW, Joyce WG. 2020.** A re-description of *Sandownia harrisi* (Testudinata: Sandownidae)

1075 from the Aptian of the Isle of Wight based on computed tomography scans. *Royal Society*

1076 *Open Science* **7:**191936.

1077 **Evers SW, Barrett PM, Benson RBJ. 2019.** Anatomy of *Rhinochelys pulchriceps*

1078 (Protostegidae) and marine adaptation during the early evolution of chelonioids. *PeerJ*

1079 **7:**e6811.

1080 **Evers SW, Neenan JM, Ferreira GS, Werneburg I, Barrett PM, Benson RBJ. 2019.**

1081 Neurovascular anatomy of the protostegid turtle *Rhinochelys pulchriceps* and comparisons of

1082 membranous and endosseous labyrinth shape in an extant turtle. *Zoological Journal of the*

1083 *Linnean Society* **187:**800–828.

1084 **Farris JS. 1972.** Estimating phylogenetic trees from distance matrices. *American Naturalist*

1085 **106:**645–668.

1086 **Ferreira GS, Lautenschlager S, Evers SW, Pfaff C, Kriwet J, Raselli I, Werneburg I. 2020.**

1087 Feeding biomechanics suggests progressive correlation of skull architecture and neck

1088 evolution in turtles. *Scientific Reports* **10:**5505.

1089 **Foth C, Evers SW, Joyce WG, Volpato V, Benson RBJ. 2019.** Comparative analysis of the

1090 shape and size of the middle ear cavity of turtles reveals no correlation with habitat ecology.

1091 *Journal of Anatomy* **235:**1078–1097.

1092 **Gaffney ES. 1972.** The systematics of the North American family Baenidae (Reptilia,

1093 Cryptodira). *Bulletin of the American Museum of Natural History* **147(5):**241–320.

1094   **Gaffney ES. 1975a.** A phylogeny and classification of the higher categories of turtles. *Bulletin*

1095   *of the American Museum of Natural History* **155(5):**387–436.

1096   **Gaffney ES. 1975b.** *Solnhofia parsonsi*, a new cryptodiran turtles from the Late Jurassic of

1097   Europe. *American Museum Novitates* **2576:**1–25.

1098   **Gaffney ES. 1976.** Cranial morphology of the European Jurassic turtles *Portlandemys* and

1099   *Plesiochelys*. *Bulletin of the American Museum of Natural History* **157(6):**487–544.

1100   **Gaffney ES. 1979a.** The Jurassic turtles of North America. *Bulletin of the American Museum of*

1101   *Natural History* **162(3):**91–136.

1102   **Gaffney ES. 1979b.** Comparative cranial morphology of Recent and fossil turtles. *Bulletin of the*

1103   *American Museum of Natural History* **164(2):**65–376.

1104   **Gaffney ES. 1990.** The comparative osteology of the Triassic turtle *Proganochelys*. *Bulletin of*

1105   *the American Museum of Natural History*, 19**4:**1–263

1106   **Gaffney ES. 1996.** The postcranial morphology of *Meiolania platyceps* and a review of the

1107   Meiolaniidae. *Bulletin of the American Museum of Natural History* **229:**1–166.

1108   **Gaffney ES, Meylan PA. 1988.** A phylogeny of turtles. In: Benton MJ, ed. *The Phylogeny and*

1109   *Classification of the Tetrapods, Volume 1: Amphibians, Reptiles, Birds, Systematics*

1110   *Association Special Volume 35A*. Oxford: Clarendon Press, 157–219.

1111   **Gaffney ES, Tong H, Meylan PA. 2006.** Evolution of the side-necked turtles: The families

1112   Bothremydidae, Euraxemydidae, and Araripemydidae. *Bulletin of the American Museum of*

1113   *Natural History* **300:**3–698.

1114   **Gaffney ES, Rich TH, Vickers-Rich P, Constantine A, Vacca R, Kool L. 2007.** *Chubutemys*,

1115   a new eucryptodiran turtles from the Early Cretaceous of Argentina, and the relationships of

1116   the Meiolaniidae. *American Museum Novitates* **3599:**1–35.

1117 **Joyce WG. 2007.** Phylogenetic relationships of Mesozoic turtles. *Bulletin of the Peabody*

1118 *Museum of Natural History* **48(1):**3–102.

1119 **Joyce WG. 2017.** A review of the fossil record of basal Mesozoic turtles. *Bulletin of the*

1120 *Peabody Museum of Natural History* **58(1):**65–113.

1121 **Joyce WG, Anquetin J. 2019.** A review of the fossil record of nonbaenid turtles of the clade

1122 Paracryptodira. *Bulletin of the Peabody Museum of Natural History* **60(2):**129–155.

1123 **Joyce WG, Lyson TR. 2015.** A review of the fossil record of turtles of the clade Baenidae.

1124 *Bulletin of the Peabody Museum of Natural History* **56(2):**147–183.

1125 **Joyce WG, Rollot Y. In Press.** An alternative interpretation of *Peltochelys duchastelii* as a

1126 paracryptodire. *Fossil Record*.

1127 **Joyce WG, Sterli J. 2012.** Congruence, non-homology, and the phylogeny of basal turtles. *Acta*

1128 *Zoologica* **93:**149–159.

1129 **Joyce WG, Chapman S, Moody RTJ, Walker CA. 2011.** The skull of the solemydid turtle

1130 *Helochelydra nopscai* from the Early Creatceous of the Isle of Wight (UK) and a review of

1131 Solemydidae. *Special Papers in Palaeontology* **86:**75–97.

1132 **Joyce WG, Sterli J, Chapman S. 2014.** The skeletal morphology of the solemydid turtle

1133 *Naomichelys speciosa* from the Early Cretaceous of Texas. *Journal of Paleontology*

1134 **88(6):**1257–1287.

1135 **Joyce WG, Rabi M, Clark JM, Xu X. 2016.** A toothed turtle from the Late Jurassic of China

1136 and the global biogeographic history of turtles. *BMC Evolutionary Biology* **16(236):**1–29.

1137 **Kluge AG, Farris JS. 1969.** Quantitative phyletics and the evolution of anurans. *Systematic*

1138 *Biology* **18:**1–32.

1139   **Lipka TR, Therrien F, Weishampel DB, Jamniczky HA, Joyce WG, Colbert MW,**

1140   **Brinkman DB. 2006.** A new turtle from the Arundel Clay Facies (Potomac Formation, Early

1141   Cretaceous) of Maryland, U.S.A. *Journal of Vertebrate Paleontology* **26(2):**300–307.

1142   **Lyson TR, Joyce WG. 2011.** Cranial anatomy and phylogenetic placement of the enigmatic

1143   turtle *Compsemys victa* Leidy, 1856. *Journal of Paleontology* **85(4):**749–801.

1144   **Milner AR. 2004.** The turtles of the Purbeck Limestone Group of Dorset, Southern England.

1145   *Palaeontology* **47(6):**1411–1467.

1146   **Nixon KC, Carpenter JM. 1993.** On outgroups. *Cladistics* **9:**413–426

1147   **Owen R. 1842.** Report on British fossil reptiles. Part II. In: *Report of the Eleventh Meeting of the*

1148   *British Association for the Advancement of Science; Held at Plymouth in July 1841.* London:

1149   Murray, 60–204.

1150   **Pérez-García A. 2014.** Revision of the poorly known *Dorsetochelys typocardium*, a relatively

1151   abundant pleurosternid turtle (Paracryptodira) in the Early Cretaceous of Europe. *Cretaceous*

1152   *Research* **49:**152–162.

1153   **Pérez-García A, Royo-Torres R, Cobos A. 2015.** A new European Late Jurassic pleurosternid

1154   (Testudines, Paracryptodira) and a new hypothesis of paracryptodiran phylogeny. *Journal of*

1155   *Systematic Palaeontology* **13(4):**351–369.

1156   **Rabi M, Zhou C-F, Wings O, Ge S, Joyce WG. 2013.** A new xinjiangchelyid turtle from the

1157   Middle Jurassic of Xinjiang, China and the evolution of the basipterygoid process in

1158   Mesozoic turtles. *BMC Evolutionary Biology* **13(203):**1–28.

1159   **Rabi M, Sukhanov VB, Egorova VN, Danilov I, Joyce WG. 2014.** Osteology, relationships,

1160   and ecology of *Annemys* (Testudines, Eucryptodira) from the Late Jurassic of Shar Teg,

1161   Mongolia, and phylogenetic definitions for Xinjiangchelyidae, Sinemydidae, and

1162   Macrobaenidae. *Journal of Vertebrate Paleontology* **34(2):**327–352.

1163   **Rieppel O. 1980.** The skull of the Upper Jurassic Cryptodire turtle *Thalassemys*, with a

1164   reconsideration of the chelonian braincase. *Palaeontographica, Abteilung A* 171:105–140.

1165   **Rollot Y, Lyson TR, Joyce WG. 2018.** A description of the skull of *Eubaena cephalica* (Hay,

1166   1904) and new insights into the cranial circulation and innervation of baenid turtles. *Journal*

1167   *of Vertebrate Paleontology* **38(3):**e1474886

1168   **Sterli J. 2010.** Phylogenetic relationships among extinct and extant turtles: the position of

1169   Pleurodira and the effects of fossils on rooting crown-group turtles. *Contributions to Zoology*

1170   **79(3):**93–106.

1171   **Sterli J, Müller J, Anquetin J, Hilger A. 2010.** The parabasisphenoid complex in Mesozoic

1172   turtles and the evolution of the testudinate basicranium. *Canadian Journal of Earth Sciences*

1173   **47:**1337–1346.

1174   **Sterli J, Pol D, Laurin M. 2013.** Incorporating phylgenetic uncertainty on phylogeny-based

1175   palaeontological dating and the timing of turtle diversification. *Cladistics* **29:**233–246.

1176   **Sukhanov VB. 2000.** Mesozoic turtles of middle and central Asia. In: Benton MJ, Shiskin MA,

1177   Unwin DM, Kurochkin EN, eds. *The Age of Dinosaurs in Russia and Mongolia.* Cambridge:

1178   Cambridge University Press, 309–367.

1179   **Zhou C-F, Rabi M. 2015.** A sinemydids turtle from the Jehol Biota provides insights into the

1180   basal divergence of crown turtles. *Scientific Reports* **5:**16299.

1181

1182   **Figure 1 Photographs of UMZC T1041, cranium of *Pleurosternon bullockii*.** A, dorsal view.

1183   B, ventral view. C, left lateral view. D, right lateral view. E, anterior view. F, posterior view.

1184   Scale bar equals 10 mm.

1185

1186   **Figure 2 Three dimensional renderings of the cranium of *Pleurosternon bullockii* (UMZC**

1187   **T1041).** A, dorsal view. B, ventral view. C, left lateral view. D, right lateral view. E, anterior

1188   view. F, posterior view. Abbreviations: bsp, parabasisphenoid; ep, epipterygoid; f, frontal; j,

1189   jugal; mx, maxilla; n, nasal; op, opisthotic; pa, parietal; pmx, premaxilla; po, postorbital; pr,

1190   prootic; prf, prefrontal; pt, pterygoid; q, quadrate; qj, quadratojugal; soc, supraoccipital; sq,

1191   squamosal. Scale bars equal 10 mm.

1192

1193   **Figure 3 Three dimensional renderings of the orbitotemporal region of *Pleurosternon***

1194   ***bullockii* (UMZC T1041).** A, anteroventral view of partial cranium. B, ventral view of partial

1195   cranium. Abbreviations: crcr, crista cranii; f, frontal; ftp, fossa temporalis; j, jugal; for, fossa

1196   orbitalis; pa, parietal; pip, processus inferior parietalis (descending process of parietal); po,

1197   postorbital; sol, sulcus olfactorius; sot, septum orbitotemporale; spp, sulcus palatino-

1198   pterygoideus. Scale bar equals 10 mm.

1199

1200   **Figure 4 Three dimensional renderings of the trigeminal region of *Pleurosternon bullockii***

1201   **(UMZC T1041).** A, anterodorsolateral view of partial right cranium. B, anterolateral view of

1202   partial right cranium. Abbreviations: ep, epipterygoid; fnt, foramen nervi trigemini (trigeminal

1203   foramen); fst, foramen stapedio-temporale; pa, parietal; pepi, processus epipterygoideus; pip,

1204   processus inferior parietalis (descending process of parietal); pppa, posterior process of parietal

1205   behind trigeminal foramen; pr, prootic; pt, pterygoid; pto-pr, prootic part of processus trochlearis

1206   oticum; pto-q, quadrate part of processus trochlearis oticum; q, quadrate; soc, supraoccipital.

1207   Scale bar equals 10 mm.

1208

1209   **Figure 5 Three dimensional renderings of aspects of the cavum acustico-jugulare and the**

1210   **inner ear capsule of *Pleurosternon bullockii* (UMZC T1041).** A, posteroventral view of partial

1211   right basicranium. B, posterolateral view of right prootic and pterygoid. C, lateral view of left

1212   prootic and opisthotic. D, medial view of left prootic and opisthotic. Abbreviations: acst, aditus

1213   canalis stapedio-temporalis; asc, anterior semicircular canal; bs-f, parabasisphenoid-facet; ccav,

1214   canalis cavernosus; ex-f, exoccipital facet; faf, fossa acustico-facialis; fja, foramen jugulare

1215   anterius; fnac, foramen nervi acustici; fov, fenestra ovalis; hac, hiatus acusticus; ica, incisura

1216   columella auris; lfng, lateral foramen nervi glossopharyngei; lsc, lateral semicircular canal;

1217   mfng, medial foramen nervi glossopharyngei; mfnf, medial foramen nervi facialis; op, opisthotic;

1218   pif, processus interfenestralis; plf, perilymphatic fossa; ppo, paroccipital process; pr, prootic; pr-

1219   lsc, prootic-part of the lateral semicircular canal; psc, posterior semicircular canal; pt, pterygoid;

1220   q, quadrate; snhy, sulcus nervi hyomandibularis; soc, supraoccipital. Scale bars equals 10 mm in

1221   A, 3 mm in B–D.

1222

1223   **Figure 6 Three dimensional renderings of the right pterygoid of *Pleurosternon bullockii***

1224   **(UMZC T1041).** A, ventral view. B, dorsal view. C, anterodorsolateral view. Abbreviations:

1225   afnv, anterior foramen for the canalis nervus vidiani; bpp-f, basisptergyoid process facet; bsp-f,

1226   parabasisphenoid facet; ccav; canalis cavernosus; crpt, crista pterygoidei; ep-f, epipterygoid

1227   facet; j-f, jugal facet; mx-f, maxilla facet; pfnv, posterior foramen for the canalis nervus vidiani;

1228   ppe, processus pterygoideus externus; pptp, posterior pterygoid process; pr-f, prootic facet; ptf,

1229   pterygoid fossa; q-f, quadrate facet; scav, sulcus cavernosus; vf, vertical flange of the external

1230   pterygoid process; vptr, ventral pterygoid ridge. Scale bar equals 3 mm.

1231

1232   **Figure 7 Three dimensional renderings of the parabasisphenoid and basipterygoid process**

1233   **of *Pleurosternon bullockii* (UMZC T1041).** A, parabasisphenoid in dorsal view. B,

1234   parabasisphenoid in ventral view. C, parabasisphenoid and left pterygoid in ventral view. D,

1235   parabasisphenoid in anterodorsal view. E, parabasisphenoid in left lateral and slight ventral view.

1236   Abbreviations: atbs, anterior tubercula basisphenoidale; bpp-df, dorsal flange of basipterygoid

1237   process; bpp-vf, ventral flange of basipterygoid process; cag, carotid groove; clp, clinoid

1238   process; cprnv, canalis pro ramo nervi vidiani; ctb, crista tuberculi basalis; ds, dorsum sellae;

1239   faccc, foramen anterius canalis carotici cerebralis; fna, foramen nervi abducentis; fpccc, foramen

1240   posterius canalis carotici cerebralis; pt-f, pterygoid facet; ptf, pterygoid fossa; rbp, retractor bulbi

1241   pit; rbs, rostrum basisphenoidale; st, sella turcica; vptr, ventral pterygoid ridge. Scale bar equals

1242   3 mm.

Figure 1

Photographs of UMZC T1041, cranium of *Pleurosternon bullockii*.

A, dorsal view. B, ventral view. C, left lateral view. D, right lateral view. E, anterior view. F, posterior view. Scale bar equals 10 mm.
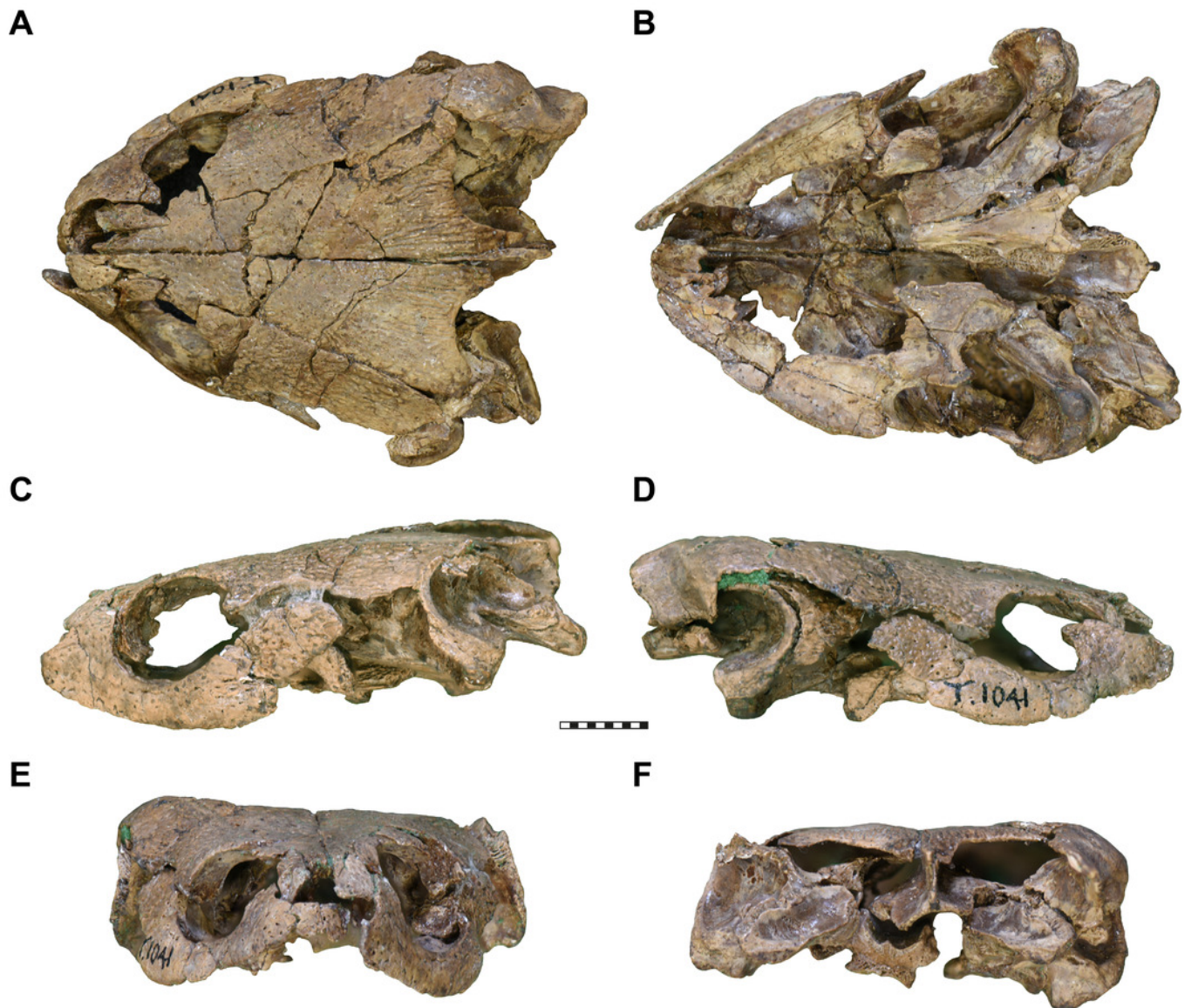
Figure 2

Three dimensional renderings of the cranium of *Pleurosternon bullockii* (UMZC T1041).

A, dorsal view. B, ventral view. C, left lateral view. D, right lateral view. E, anterior view. F, posterior view. Abbreviations: bsp, parabasisphenoid; ep, epipterygoid; f, frontal; j, jugal; mx, maxilla; n, nasal; op, opisthotic; pa, parietal; pmx, premaxilla; po, postorbital; pr, prootic; prf, prefrontal; pt, pterygoid; q, quadrate; qj, quadratojugal; soc, supraoccipital; sq, squamosal. Scale bars equal 10 mm.
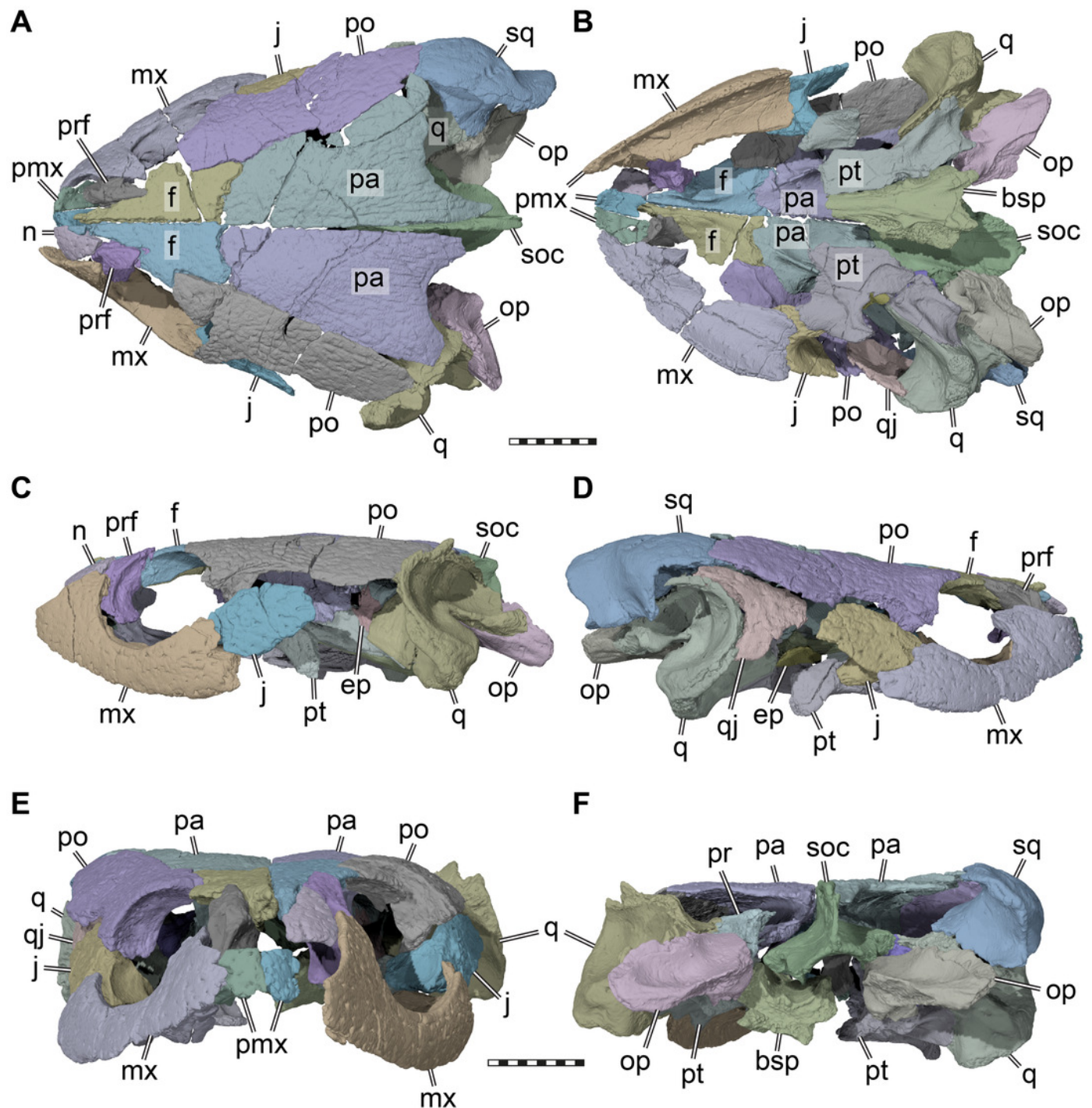
Figure 3

Three dimensional renderings of the orbitotemporal region of *Pleurosternon bullockii* (UMZC T1041).

A, anteroventral view of partial cranium. B, ventral view of partial cranium. Abbreviations: crcr, crista cranii; f, frontal; ftp, fossa temporalis; j, jugal; for, fossa orbitalis; pa, parietal; pip, processus inferior parietalis (descending process of parietal); po, postorbital; sol, sulcus olfactorius; sot, septum orbitotemporale; spp, sulcus palatino-pterygoideus. Scale bar equals 10 mm.
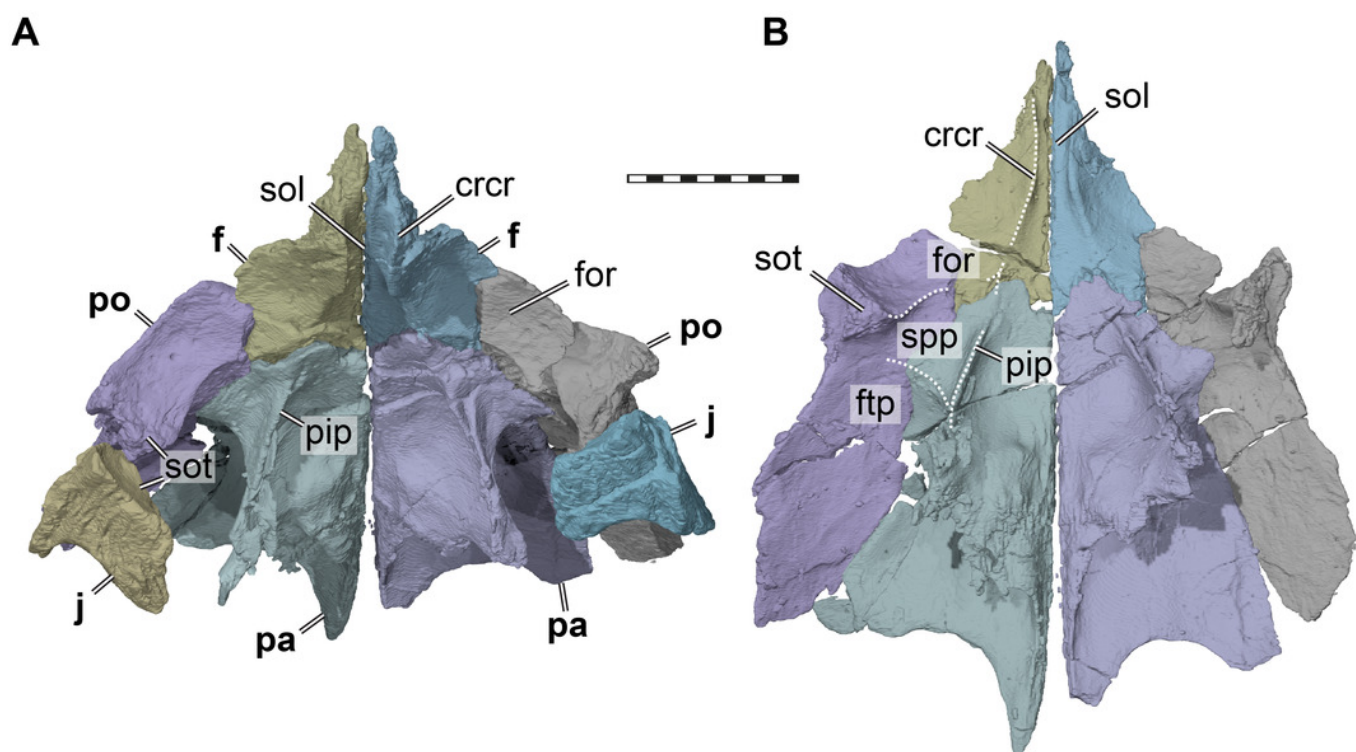
Figure 4

Three dimensional renderings of the trigeminal region of *Pleurosternon bullockii* (UMZC T1041).

A, anterodorsolateral view of partial right cranium. B, anterolateral view of partial right cranium. Abbreviations: ep, epipterygoid; fnt, foramen nervi trigemini (trigeminal foramen); fst, foramen stapedio-temporale; pa, parietal; pepi, processus epipterygoideus; pip, processus inferior parietalis (descending process of parietal); pppa, posterior process of parietal behind trigeminal foramen; pr, prootic; pt, pterygoid; pto-pr, prootic part of processus trochlearis oticum; pto-q, quadrate part of processus trochlearis oticum; q, quadrate; soc, supraoccipital. Scale bar equals 10 mm.
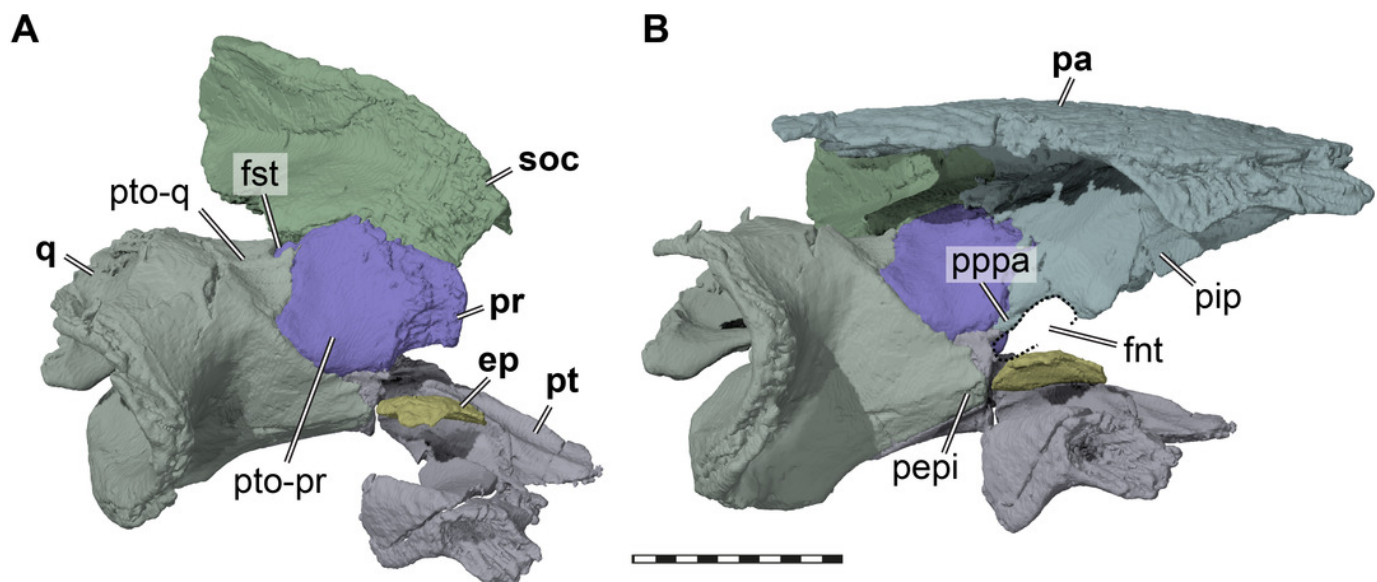
Figure 5

Three dimensional renderings of aspects of the cavum acustico-jugulare and the inner ear capsule of *Pleurosternon bullockii* (UMZC T1041).

A, posteroventral view of partial right basicranium. B, posterolateral view of right prootic and pterygoid. C, lateral view of left prootic and opisthotic. D, medial view of left prootic and opisthotic. Abbreviations: acst, aditus canalis stapedio-temporalis; asc, anterior semicircular canal; bs-f, parabasisphenoid-facet; ccav, canalis cavernosus; ex-f, exoccipital facet; faf, fossa acustico-facialis; fja, foramen jugulare anterius; fnac, foramen nervi acustici; fov, fenestra ovalis; hac, hiatus acusticus; ica, incisura columella auris; lfng, lateral foramen nervi glossopharyngei; lsc, lateral semicircular canal; mfng, medial foramen nervi glossopharyngei; mfnf, medial foramen nervi facialis; op, opisthotic; pif, processus interfenestralis; plf, perilymphatic fossa; ppo, paroccipital process; pr, prootic; pr-lsc, prootic-part of the lateral semicircular canal; psc, posterior semicircular canal; pt, pterygoid; q, quadrate; snhy, sulcus nervi hyomandibularis; soc, supraoccipital. Scale bars equals 10 mm in A, 3 mm in B–D.
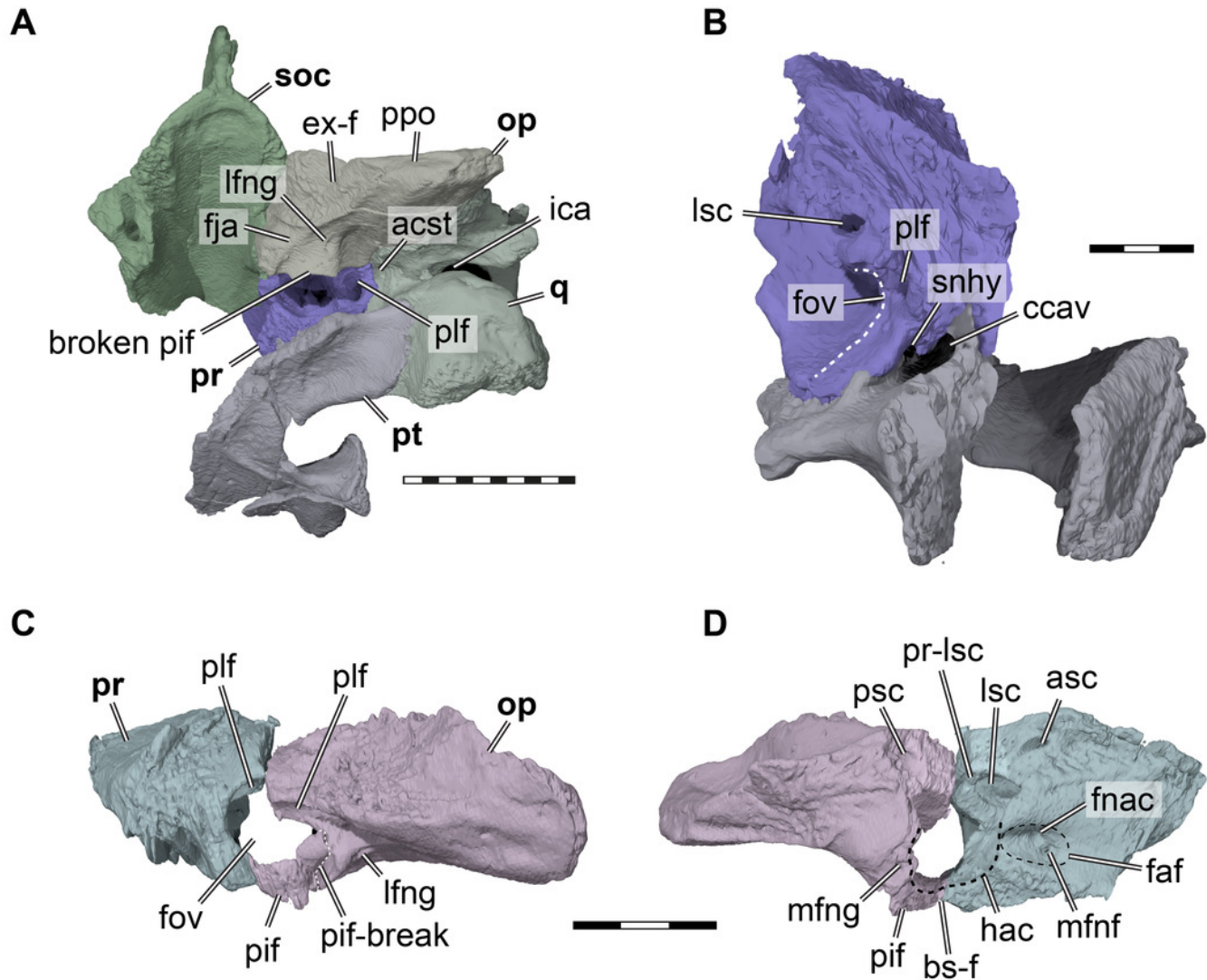
Figure 6

Three dimensional renderings of the right pterygoid of *Pleurosternon bullockii* (UMZC T1041).

A, ventral view. B, dorsal view. C, anterodorsolateral view. Abbreviations: afnv, anterior foramen for the canalis nervus vidiani; bpp-f, basisptergyoid process facet; bsp-f, parabasisphenoid facet; ccav; canalis cavernosus; crpt, crista pterygoidei; ep-f, epipterygoid facet; j-f, jugal facet; mx-f, maxilla facet; pfnv, posterior foramen for the canalis nervus vidiani; ppe, processus pterygoideus externus; pptp, posterior pterygoid process; pr-f, prootic facet; ptf, pterygoid fossa; q-f, quadrate facet; scav, sulcus cavernosus; vf, vertical flange of the external pterygoid process; vptr, ventral pterygoid ridge. Scale bar equals 3 mm.
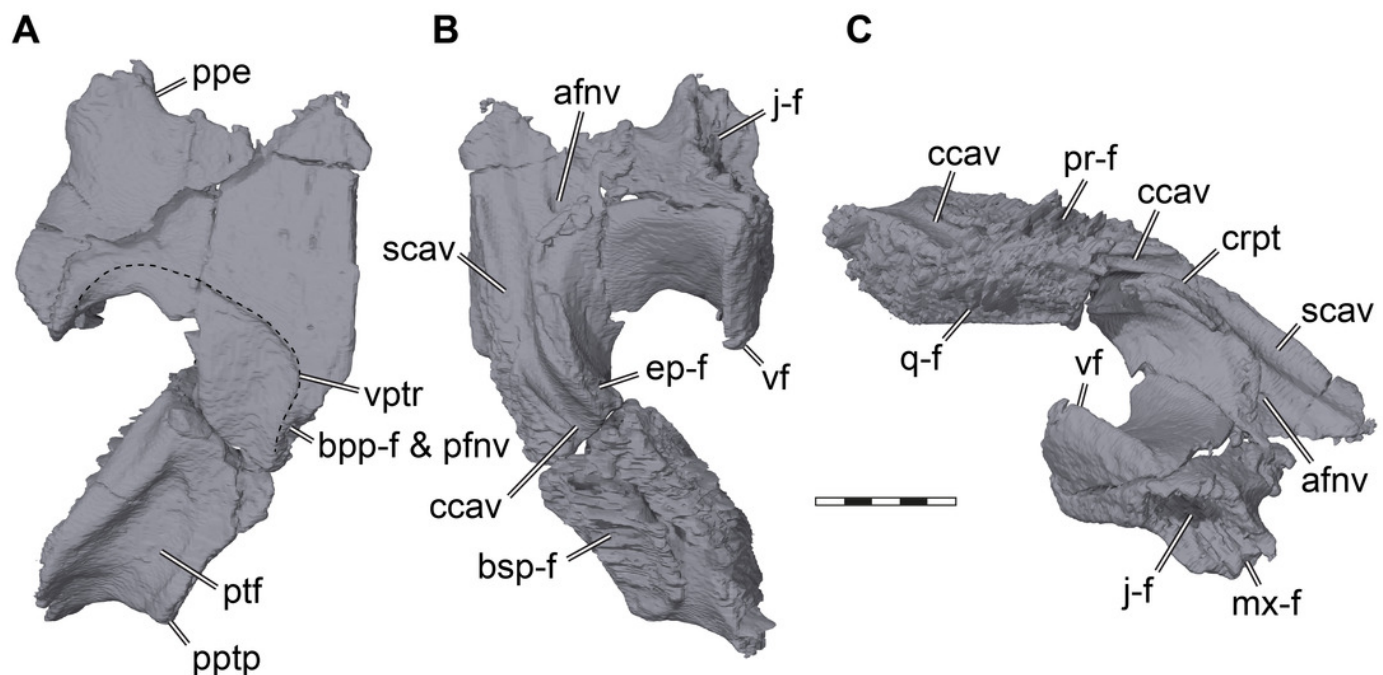
Figure 7

Three dimensional renderings of the parabasisphenoid and basipterygoid process of Pleurosternon bullockii (UMZC T1041).

A, parabasisphenoid in dorsal view. B, parabasisphenoid in ventral view. C, parabasisphenoid and left pterygoid in ventral view. D, parabasisphenoid in anterodorsal view. E, parabasisphenoid in left lateral and slight ventral view. Abbreviations: atbs, anterior tubercula basisphenoidale; bpp-df, dorsal flange of basipterygoid process; bpp-vf, ventral flange of basipterygoid process; cag, carotid groove; clp, clinoid process; ctb, crista tuberculi basalis; ds, dorsum sellae; faccc, foramen anterius canalis caroticus cerebralis; fna, foramen nervi abducentis; fpccc, foramen posterius canalis caroticus cerebralis; fprnv, foramen pro ramo nervi vidiani; pt-f, pterygoid facet; ptf, pterygoid fossa; rbp, retractor bulbi pit; rbs, rostrum basisphenoidale; st, sella turcica; vptr, ventral pterygoid ridge. Scale bar equals 3 mm.